Structure of the $N = 126$ nuclide ^{212}Rn: Valence and core excited configurations

G. D. Dracoulis,[1,*] G. J. Lane,[1] A. P. Byrne,[1,2] P. M. Davidson,[1] T. Kibédi,[1] P. H. Nieminen,[1,†] H. Watanabe,[1,‡] A. N. Wilson,[1,2] H. L. Liu,[3] and F. R. Xu[3]

[1]*Department of Nuclear Physics, Research School of Physics and Engineering, Australian National University, Canberra, Australian Capital Territory 0200, Australia*

[2]*Department of Physics, The Faculties, Australian National University, Canberra, Australian Capital Territory 0200, Australia*

[3]*School of Physics, Peking University, Beijing 100871, People's Republic of China*

(Received 22 July 2009; revised manuscript received 23 September 2009; published 30 November 2009)

The level scheme of ^{212}Rn has recently been expanded and extended to spins of $\sim 39\hbar$ and excitation energies of about 13 MeV using the ^{204}Hg(^{13}C,5n)^{212}Rn reaction and γ-ray spectroscopy. Time-correlated techniques were used to obtain channel selectivity and improved sensitivity. New γ-ray branches from states associated with valence proton configurations as well as a number of new states below the 22^+ isomer have been identified. The excitation energy of the 22^+ core excited isomer itself has been established through the observation of several branches parallel to the main decay, implying a transition energy of 7.6 keV for the previously unobserved decay to the 20^+_2 state. The level scheme above the 22^+ isomer includes two new isomers with $\tau = 25(2)$ ns and $\tau = 12(2)$ ns placed at 12,211 and 12,548 keV, respectively. These are attributed to configurations involving triple neutron core excitations coupled to the aligned valence protons. The results are compared to semiempirical shell-model calculations, which can account for many of the states observed, with considerable precision for the valence proton configurations but with significant energy discrepancies for some core excited configurations. Calculations within the deformed independent particle model (DIPM) have also been carried out for the main core excited configurations at high spin and compared with both experiment and the empirical shell-model approach. The possible sources of discrepancies in both approaches are discussed, and it is suggested that anomalously low excitation energies are predicted for specific configurations in the DIPM.

DOI: 10.1103/PhysRevC.80.054320 PACS number(s): 21.10.Tg, 21.60.Cs, 23.20.Lv, 27.80.+w

I. INTRODUCTION

The identification of excited states in nuclei close to the $Z = 82$, $N = 126$ double-shell closure has been an important part of the development of the understanding of the structure of heavy nuclei. The nuclide ^{212}Rn, in particular, with its relatively simple structure of a closed neutron core and four valence protons, is attractive as a testing ground for the study of both low- and high-spin states [1–7]. The principal interests have been to develop shell-model approaches and probe their limit of applicability and, from another point of view, to address the question of whether deformation plays a role. The latter is a natural expectation given that increasing numbers of particles congregate near the nuclear equator as high angular momentum states are formed by the mutual alignment of the spins of individual nucleons. This expectation is captured in the deformed independent particle model approach [8,9].

From the shell-model viewpoint, the main ingredients controlling the formation of the yrast line seem to be the attractive proton-neutron residual interactions acting between mutually aligned particles and the nonlinear particle-octupole-vibration coupling, which favors specific (multiparticle) proton and neutron configurations [10]. The attractive interactions offset the cost in energy incurred in promoting neutrons out of the core so as to gain angular momentum by populating the high-j orbitals above the neutron Fermi surface, the prime method of making higher spins once the angular momentum available from the valence protons is exhausted.

The energy favoring of a particular class of configuration to form high-spin states is also manifested, in general, in the presence of isomers. In ^{212}Rn, early studies identified high-spin yrast isomers up to spins of $30\hbar$ [1,2] and excitation energies of about 8.5 MeV, some involving double neutron-core excitations. A $J^\pi = 33^-$ isomer and high-lying γ-ray transitions were subsequently observed in work that was a precursor to the present study [3]. Yrast states with related configurations have also been identified in ^{211}Rn and ^{210}Rn [11,12]. In ^{212}Rn, states with higher spin than $33\hbar$ can be formed, in principle, with relatively simple configurations by combining the valence protons and other double neutron-core excitations to exploit further the $g_{9/2}$, $i_{11/2}$, and $j_{15/2}$ orbitals above the neutron Fermi surface. The lowest of these are likely to involve proton components such as the $(h^3_{9/2}i_{13/2})_{17^-}$ and $(h^2_{9/2}i^2_{13/2})_{20^+}$ configurations coupled to two neutron-core excitations, for example, $(p^{-2}_{1/2}g_{9/2}i_{11/2})_{10^+}$ or $(p^{-2}_{1/2}j^2_{15/2})_{14^+}$, giving states with $J \sim 34\hbar$. At that stage, triple neutron-core excitations might also become competitive, with the maximum spins available from energetically favored configurations being about $40\hbar$. The present study of ^{212}Rn was aimed at both a more comprehensive study of the level scheme and the identification of states in this limiting region of angular momentum. A

*george.dracoulis@anu.edu.au

†Present address: Department of Physics, University of Jyväskylä, PO Box 35, FI-40014 Jyväskylä, Finland.

‡Present address: Nuclear Physics Research Division, RIKEN Nishina Center for Accelerator-Based Science, 2-1 Hirosawa, Wako 351-0198, Japan.

number of aspects of the present results on the new high-spin isomers identified, and their configurations, were published recently [13]. More information on the spectroscopic results and assignments relevant to the earlier letter is provided in this article, in addition to a comparison between the shell-model and deformed independent particle model approaches. Results on the $N = 126$ nuclide, ^{210}Po, obtained in the same measurements, have also been published [14].

II. EXPERIMENTAL DESIGN AND DETAILS

The results were obtained using the (^{13}C,5n) reaction on ^{204}Hg. Two sets of measurements were made using similar beam-target conditions but with different configurations for the γ-ray array, CAESAR. An oxide target enriched in ^{204}Hg was used for both, with a pulsed beam of ^{13}C at 89 MeV provided by the Australian National University 14UD Pelletron accelerator. Pulses of about 1 ns in width were separated by 856 ns, a configuration chosen to match the lifetimes of the 22^+ and 30^+ isomers. (The low-lying 8^+ isomer has a longer lifetime of 1.2 μs.) The energy was chosen to enhance the high-spin population in the ^{204}Hg (^{13}C,5n)^{212}Rn reaction, being above the peak of the cross section for the 5n evaporation channel and therefore at the expense of increased contamination from the 6n channel leading to ^{211}Rn. The nominal maximum angular momentum input (sharp cutoff) is about 40$\hbar$. Our previous measurements [3] used this reaction at lower energies and also the ^{198}Pt(^{18}O,4n)^{212}Rn. The latter has a more convenient target but not as high an angular momentum input.

In the first set of measurements the array comprised six hyperpure Ge detectors and one LEPS detector for enhanced low-energy efficiency. The six Compton suppressed detectors in CAESAR are arranged in the vertical plane, in pairs, at angles with respect to the beam direction of $\pm 97^\circ$, $\pm 148^\circ$, and $\pm 48^\circ$, allowing γ-ray anisotropies to be measured. In the second set of measurements, the array was augmented with the addition of three large-volume Ge detectors (Compton suppressed and 80% efficient) and an additional LEPS detector, all in the horizontal plane.

Gamma-γ-time matrices were constructed from these data to establish the coincidence relationships. Where possible, additional time conditions were used to select γ rays feeding or following isomers. Lifetime information was obtained by projecting intermediate-time spectra from γ-γ-time cubes with gates on γ rays above and below the state of interest as well as from the γ-ray-time data with respect to the nanosecond-pulsed beams.

Analysis of the data from the second experiment was also aimed at providing angular anisotropy information to constrain multipolarities for transitions above the 22^+ isomer. This was accomplished by constructing three matrices, with transitions observed in any of the three pairs of six detectors in the vertical plane (defining three angles with respect to the beam axis), on one axis, with any delayed transitions observed in the other eight large detectors. Gates were then set on the delayed transitions, beginning with the main cascade transitions below the 22^+ isomer and progressively moving up in the level scheme to isolate specific transitions above the 30^+ isomer, without contamination. As will be evident later, this also allowed several independent determinations of the anisotropies of the higher transitions and the isolation of cases where specific transitions are contaminated by γ rays of similar energy, lower in the level scheme.

Spectra constructed from such matrices allowed three-point anisotropies to be determined. (Note that these will be indicative of spin differences but are not sufficient to extract precise mixing ratios.) The angle and energy-dependent relative efficiencies required for the anisotropy determination were internally calibrated using the broad spectrum of lines produced in activity. The overall relative efficiency was determined using standard sources.

III. RESULTS AND LEVEL SCHEME

Transitions assigned to ^{212}Rn, including those reported in Ref. [13], are listed in Table I together with their placement in the scheme, relative intensities, and, where available, anisotropies, as observed in the present experiments. The anisotropies are given in terms of the normalized coefficient in a fit to an expansion, up to second order, in the Legendre polynomial.

The level scheme is presented in two main parts: Fig. 1 includes states up to the 22^+ isomer at 6174 keV, while higher states are shown in Fig. 2. Stuchbery *et al.* [4] summarized the properties of states up to the 22^+ isomer as known at that time, and additional transitions were assigned by Lönnroth *et al.* [5]. In relation to those works, nearly all transitions have been independently confirmed and about 20 new transitions placed in this part of the level scheme. These transitions confirm the levels previously assigned and result in the assignment of five new states as well as in the definition of the excitation energy of the 22^+ isomer itself, as discussed in the following. The only cases in which no significant new information or specific confirmation was found are for the 2306-keV state and the associated 804.8-keV transition, which is only known from β decay, and the 1002.1-keV transition, which defines a state at 2696 keV but is observed only weakly in the present reaction.

Transitions of note, in addition to those that define new states, include the 1066.4- and 644.5-keV $E3$ decays from the 11^- isomer at 2761 keV. The former had been observed previously [5], but its intensity had not been precisely defined, while the weaker 644.5-keV branch is new. The 1705-keV $E2$ transition that connects the 19^- core excited state with the 17^- valence proton state is observed for the first time, and as reported in Ref. [13], numerous decays from the 22^+ excited state have been assigned. Their decay properties will be discussed in the following section.

Figure 3 gives representative spectra obtained with gates on some of the weaker decay paths, populated in the out-of-beam time region. The spectrum gated on the 345-keV transition connecting the 19^- state to the 20^+ state at 5427 keV shows the strong 1360-keV transition, the main branch from that state, and also the 775- and 1291-keV γ rays, placed as transitions from a new state at 5357 keV. The 70-keV connecting transition is inferred, but the γ ray was not observed directly, partly

TABLE I. Energies, intensities, angular distributions, and initial and final energies, spins, and parities of transitions assigned to ^{212}Rn.

E_γ[a]	I_γ[a]	A_2/A_0[b]	E_i	E_f	J_i^π	J_f^π
7.6	*423(9)*		6174.2	6166.4	22^+	20^+
15.5	*68(5)*		7878.3	7862.8	27^-	26^-
20.0	*16(3)*		3297.6	3277.9	12^+	11^+
21.9	*40(7)*		8579.2	8557.3	30^+	$28^{(-)}$
54.2	6.7(8)		1693.9	1639.7	8^+	6^+
59.2	*57(6)*		7878.3	7819.1	27^-	26^-
59.8	*155(23)*		3357.3	3297.6	14^+	12^+
67.9	8.7(11)		4134.4	4066.4	16^-	17^-
70.0	*24(4)*		5426.9	5357.0	20^+	(18^+)
75.7	20.5(11)		4066.4	3990.7	17^-	15^-
81.9	*46(6)*		8579.2	8497.3	30^+	28^+
92.4	*5(1)*		11,354.6	11,262.2	35^-	35^-
105.8	81.5(28)		2760.5	2654.7	11^-	10^+
118.0	2.3(4)		10,961.4	10,843.4	(33)	(32)
120.7	3.4(8)		2881.1	2760.5	12^+	11^-
138.3	377(24)		1639.7	1501.4	6^+	4^+
143.7	5.1(6)		4134.4	3990.7	16^-	15^-
158.4	1.7(3)	0.29(23)	12,211.3	12,052.7	$(37^{(-)})$	(37)
179.3	4.5(5)	−0.40(20)	11,354.6	11,175.4	35^-	(34)
195.5	2.2(4)		8557.3	8362.0	$28^{(-)}$	(27^-)
206.6	3.4(3)		2967.2	2760.5	(12^+)	11^-
211.8	5.1(3)		3277.9	3066.1	11^+	10^+
214.0	12.3(8)	−0.12(11)	11,175.4	10,961.4	(34)	(33)
226.4	553(6)		2881.1	2654.7	12^+	10^+
227.7	751(6)		1501.4	1273.7	4^+	2^+
231.5	10(2)		3297.6	3066.1	12^+	10^+
255.6	3.4(9)		3990.7	3735.0	15^-	13^-
285.4	5.0(6)	−0.65(23)	12,165.7	11,880.3	(36)	(35)
294.5	5.0(6)	−0.31(23)	7819.1	7524.6	26^-	25^-
336.3	6.8(6)	−0.44(15)	12,547.6	12,211.3	(38^+)	(37^-)
344.8	26.7(20)		5771.4	5426.9	19^-	20^+
353.7	26.3(25)	0.59(14)	8932.9	8579.2	30^+	30^+
353.8	10.4(30)		7878.3	7524.6	27^-	25^-
356.3	8.1(7)	−0.53(13)	7177.7	6821.4	$24^{(+)}$	23^+
372.3	15.2(17)		6166.4	5794.6	20^+	(19^+)
382.6	21.5(16)	0.21(9)	7524.6	7142.0	25^-	25^-
395.0	360(9)		6166.4	5771.4	20^+	19^-
402.5	8.1(14)		6174.2	5771.4	22^+	19^-
406.6	15.5(6)	−0.15(13)	10,102.4	9695.8	(32)	33^-
416.2	∼0.9		4151.1	3735.0	15^-	13^-
416.3	83(4)		3297.6	2881.1	12^+	12^+
422.0	33.2(22)		2115.9	1693.9	8^+	8^+
432.5	24.3(17)	0.11(9)	7142.0	6709.2	25^-	23^+
447.8	45.0(28)		4582.1	4134.4	17^-	16^-
449.2	10.3(15)	−0.23(20)	9028.4	8579.2	31	30^+
472.8	7.6(22)	−0.38(20)	11,827.4	11,354.6	36	35^-
476.2	570(11)		3357.3	2881.1	14^+	12^+
483.7	24.9(13)	0.22(11)	8362.0	7878.3	(27^-)	27^-
515.7	225(6)		4582.1	4066.4	17^-	17^-
531.7	227(6)		5113.8	4582.1	18^-	17^-
535.0	57.2(29)	−0.50(6)	6709.2	6174.2	23^+	22^+
537.1	71.6(37)		3297.6	2760.5	12^+	11^-
615.2	8.1(10)	−0.47(18)	10,124.6	9509.4	32^+	31^+
619.0	43.2(25)	−0.11(7)	8497.3	7878.3	28^+	27^-
623.3	19.1(25)		3277.9	2654.7	11^+	10^+
628.9	∼2		3510.2	2881.1	(13^+)	12^+

TABLE I. (*Continued*.)

E_γ[a]	I_γ[a]	A_2/A_0[b]	E_i	E_f	J_i^π	J_f^π
633.4	607(17)		3990.7	3357.3	15^-	14^+
640.5	14.1(22)		3998.0	3357.3	(14^-)	14^+
642.7	15.0(13)	−0.71(14)	11,262.2	10,619.5	35^-	34^-
644.5	3.1(6)		2760.5	2115.9	11^-	8^+
647.2	20.4(16)	−0.80(10)	6821.4	6174.2	23^+	22^+
657.6	429(10)		5771.4	5113.8	19^-	18^-
677.1	72.3(49)	−0.56(7)	7819.1	7142.0	26^-	25^-
679.0	59.3(47)	−0.17(6)	8557.3	7878.3	$28^{(-)}$	27^-
698.1	15.7(19)	0.25(16)	12,052.7	11,354.6	(37)	35^-
700.9	322(10)	0.10(4)	8579.2	7878.3	30^+	27^-
709.1	88.8(42)		4066.4	3357.3	17^-	14^+
720.8	88.7(43)	−0.38(6)	7862.8	7142.0	26^-	25^-
735.1	34.7(20)	−0.62(13)	11,354.6	10,619.5	35^-	34^-
736.3	322(12)	0.09(4)	7878.3	7142.0	27^-	25^-
739.7	35.4(25)		6166.4	5426.9	20^+	20^+
747.3	55.4(28)		6174.2	5426.9	22^+	20^+
774.8	12.1(22)		5357.0	4582.1	(18^+)	17^-
778.3	5.1(14)		4929.3	4151.1	(16^-)	15^-
793.7	14.9(25)		4151.1	3357.3	15^-	14^+
804.8[c]			2306.3	1501.4	(6^+)	4^+
843.0	3.7(5)		11,462.5	10,619.5	(35)	34^-
844.5	22.2(42)		5426.9	4582.1	20^+	17^-
856.7	43.8(30)	0.33(18)	12,211.3	11,354.6	(37)	35^-
859	4.4(16)		10,961.4	10,102.4	(33)	(32)
862.8	10.4(8)		4929.3	4066.4	(16^-)	17^-
865.0	23.9(8)		5794.6	4929.3	(19^+)	(16^+)
867.5	21.1(23)	−1.3(2)	9446.6	8579.2	31^+	30^+
923.7	82.1(25)	−0.73(6)	10,619.5	9695.8	34^-	33^-
930.3	39.3(16)	−0.83(6)	9509.4	8579.2	31^+	30^+
938.3	13.5(20)		4929.3	3990.7	(16)	15^-
949.5	9.9(25)		12,211.3	11,262.2	(37^-)	35^-
950.3	23.6(25)		3066.1	2115.9	10^+	8^+
960.8	839(18)		2654.7	1693.9	10^+	8^+
967.8	496(10)	0.19(3)	7142.0	6174.2	25^-	22^+
974.4	10.1(20)		3735.0	2760.5	13^-	11^-
979.6	18.3(22)		5113.8	4134.4	18^-	16^-
1002.1	8.7(17)		2696.0	1693.9	(8)	8^+
1029.2	29.1(16)	−0.49(11)	9608.4	8579.2	31	30^+
1047.4	129(10)		5113.8	4066.4	18^-	17^-
1066.4	7.0(8)		2760.5	1693.9	11^-	8^+
1116.6	179(6)	0.47(6)	9695.8	8579.2	33^-	30^+
1164	3.5(9)		13,375.0	12,211.3	(38)	(37^-)
1212.3	4.8(9)		5794.6	4582.1	(19^+)	17^-
1233.3	8.5(20)		13,444.6	12,211.3	(39)	(37)
1260.8	10.7(16)	−0.04(37)	11,880.3	10,619.5	(35)	34^-
1273.7	1000(23)		1273.7	0.0	2^+	0^+
1290.5	17.4(25)		5357.0	4066.4	(18^+)	17^-
1334.0	13.3(14)	−0.14(14)	10,843.4	9509.4	(32)	31^+
1355.4	13.2(13)	0.34(19)	8497.3	7142.0	28^+	25^-
1360.3	124(8)		5426.9	4066.4	20^+	17^-
1390.2	4.0(10)		11,086.0	9695.8	(34)	33^-
1658.4	7.9(14)		11,354.6	9695.8	35^-	33^-
1705.1	3.7(6)		5771.4	4066.4	19^-	17^-

[a]Unobserved transitions are given in italics with total intensities.

[b]From a three-point anisotropy.

[c]Transition is known from decay studies but was not observed in this work.

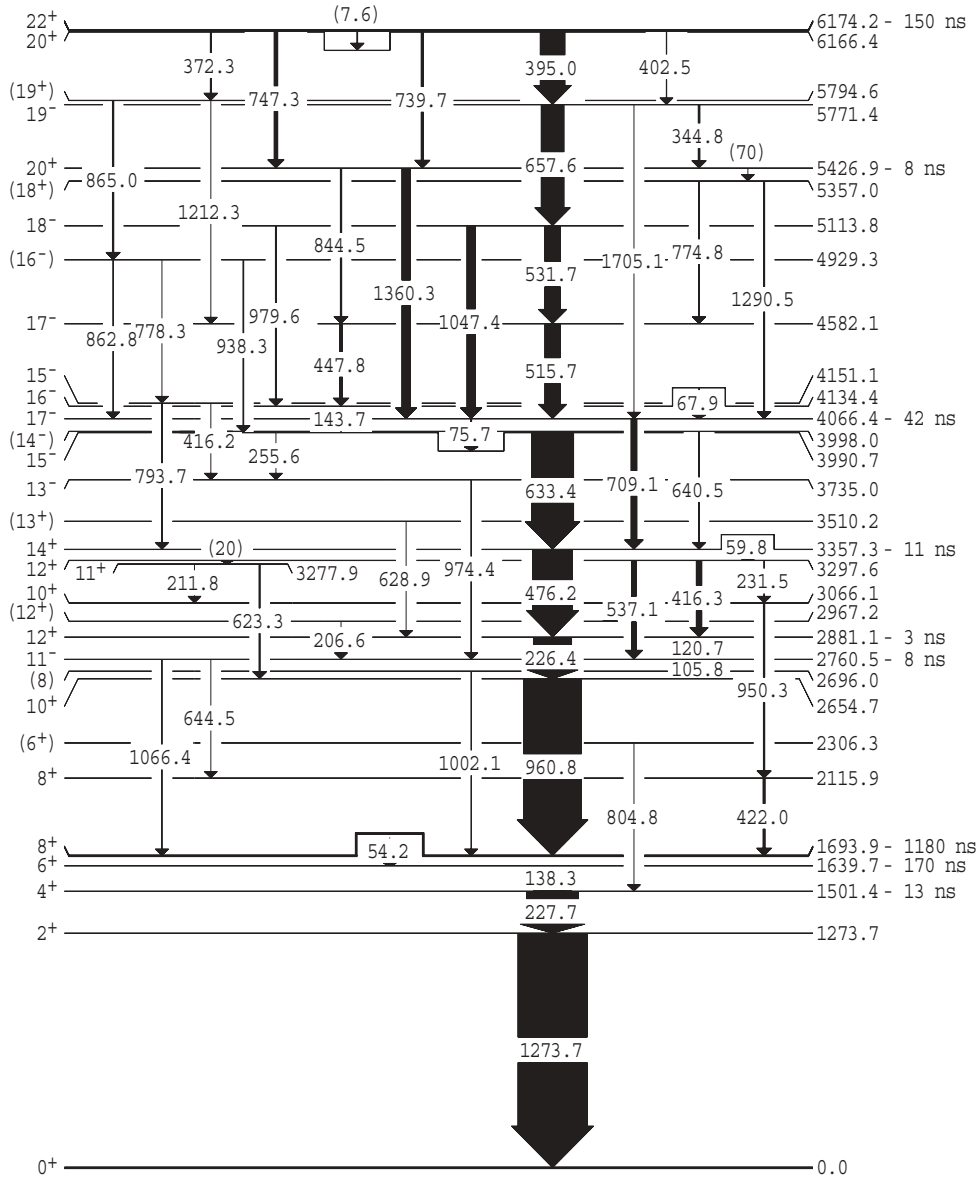

FIG. 1. Partial level scheme of ^{212}Rn showing states up to the 22^+ isomer. (See Fig. 2 for the upper part of the scheme.) The arrow widths are approximately proportional to the relative γ-ray intensities. Mean lives for the isomeric states are also indicated.

because its intensity would be low (since it would be a highly converted $E2$ transition) and partly because it overlaps with the x rays from the target. The spectrum obtained with a gate on the 422-keV branch from the 2115.9 8_2^+ state in Fig. 3 shows strong 212-, 232-, and 950-keV transitions, defining several new paths parallel to the main (226–961 keV) cascade. (Note that the 961-keV transition is present in the 422-keV gate, even though these two are in parallel, because of an unplaced transition with an energy of 422.3 keV, apparently in coincidence with the 961-keV γ ray.)

The 372-keV gated spectrum in Fig. 3 shows that the 372-keV transition is parallel to the 395-keV transition and that it feeds the new 5795-keV state, which has several decay paths, via the 865- and 863-keV cascade and the 1212-keV transition to the 17^- state at 4582 keV.

A. Energy and decay properties of the 22^+ isomer

This isomer was originally placed by Horn *et al.* [1] at an energy of $6167.3 + \Delta$ keV and was assumed to connect to the main sequence by an unobserved low-energy transition. New branches from the 20_2^+ state and from the isomer itself, which allow the energy of the 22^+ state, and therefore the energy of the unobserved transition that connects them, to be defined, were reported in Ref. [13], as shown in the level scheme (Fig. 1). (Note that the reevaluation of excitation energies from the present measurements, which include a number of new transitions, leads to the slightly lower excitation energy of 6166.4 keV for the 20_2^+ state.)

The main transitions of interest are shown in Fig. 4. (They are included in the level scheme of Fig. 1 and repeated in Fig. 2.) In addition to the strong 395.0-keV transition known

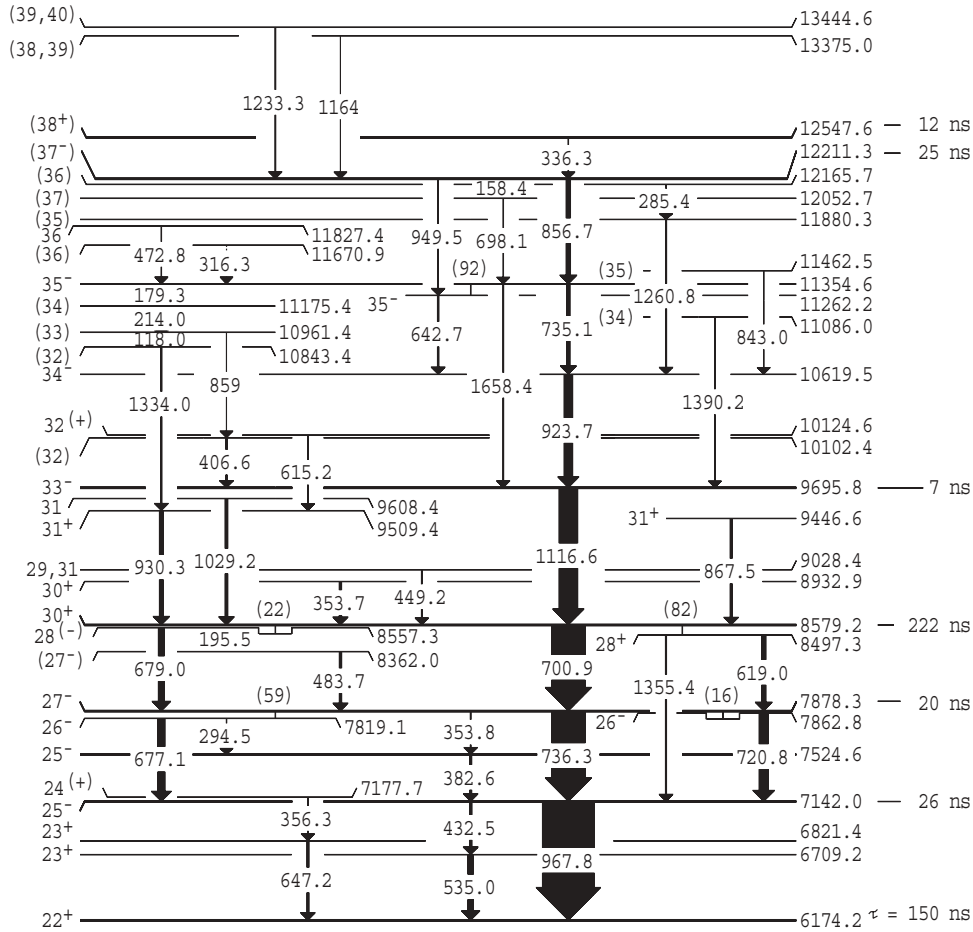

FIG. 2. Partial level scheme of ^{212}Rn showing states above the 22^+ isomer.

before, a $20_2^+ \rightarrow 20_1^+$ was assigned in Ref. [5] (although our energy is 739.7 keV, rather than 741.9 keV), and we observe a new 372.3-keV decay. Two other transitions with energies of 402.5 and 747.3 keV are placed in this work as decays from the isomer directly to the yrast 19^- (core excited) state at 5771.4 keV and to the 20_1^+ state at 5426.9 keV, respectively. The energy of the 22^+ isomer is defined as 6174.2(3) keV, consistent with the difference in energies of the pair of γ rays at 395.0 and 402.5 keV and with the pair at 739.7 and 747.3 keV, which give a value of $\Delta = 7.6(3)$ keV.

All these transitions can be placed unambiguously through a combination of time-correlated gates. For example, the prompt coincidence spectrum for the 403-keV transition given in Fig. 4 (bottom) indicates that it feeds the 19^- state but that it is parallel to the 395-keV transition; the spectra with prompt and early gates on the 747-keV transition place it as a direct feed to the lower 20^+ state but also below the 22^+ isomer. The spectrum of transitions following the 968-keV transition (Fig. 4, top) that directly feeds the 22^+ isomer confirms the new decays. (In these particular cases, "prompt" refers to a $\pm$150-ns relative time condition, while the "delayed" and "early" spectra are constrained with relative time gates of +150 to +850 ns and −150 to −850 ns. Different time conditions were used in other parts of the scheme, depending on the lifetimes involved.)

B. States above the 22^+ isomer

The level scheme above the 22^+ isomer, as discussed in Ref. [13], is shown in Fig. 2. The only modification compared to Ref. [13] is the assignment of $J^\pi = 28^{(-)}$ to the 8557.3-keV state, rather than (28^+), as will be discussed in a subsequent section.

There are effectively four parallel paths connecting states between the 25-ns isomer at 12,211 keV and the 30^+, 220-ns isomer at 8579 keV, including a path via low-energy γ rays and then the 1334- and 930-keV cascades, as indicated on the left of the level scheme (Fig. 2). Similarly, parallel paths are established across all the main cascade transitions lower in this part of the scheme such as the 432.5/535.0-keV pair across the 967.8-keV transition and the 353.8/382.6-keV pair across the 736.3-keV transition. There are also several cases in which the coincidence relationships imply unobserved low-energy transitions such as a connection (58 keV) from the 27^- isomer to the 7819.1-keV state, which decays via the 677.1- and 294.5-keV transitions; a 22-keV transition connecting the 30^+ isomer to a state at 8557.3 keV; an 82-keV transition from the same isomer to the 8497.3-keV state; and a 16-keV transition from the 27^- isomer to the 7862.8-keV state. Each of these branches is significant for the deduction of the transition strengths for the main decays.

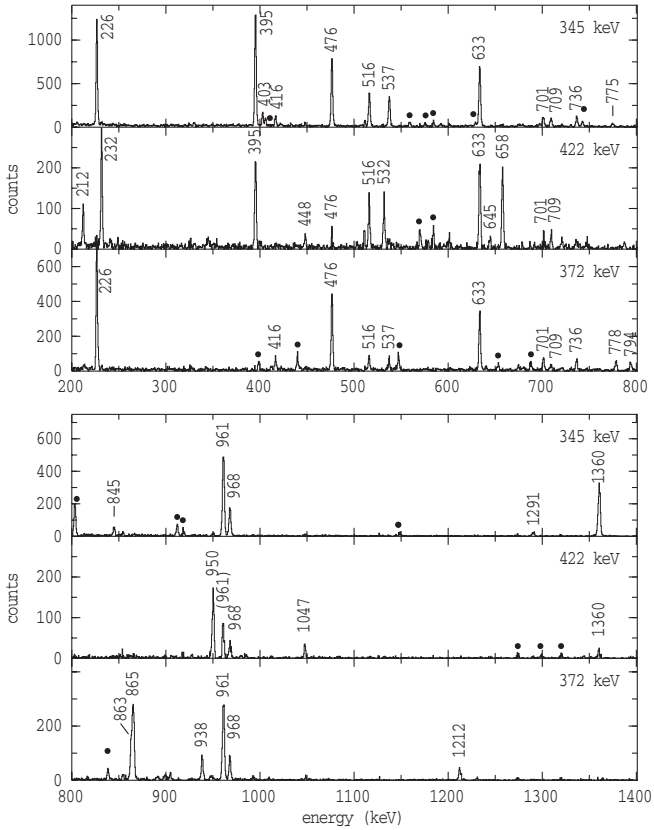

FIG. 3. Coincidence γ-ray spectra with energy gates as indicated and with an absolute time gate to select transitions between beam pulses. The upper and lower sets of panels cover contiguous low- and high-energy regions of the spectra. Known contaminants are indicated by solid circles.

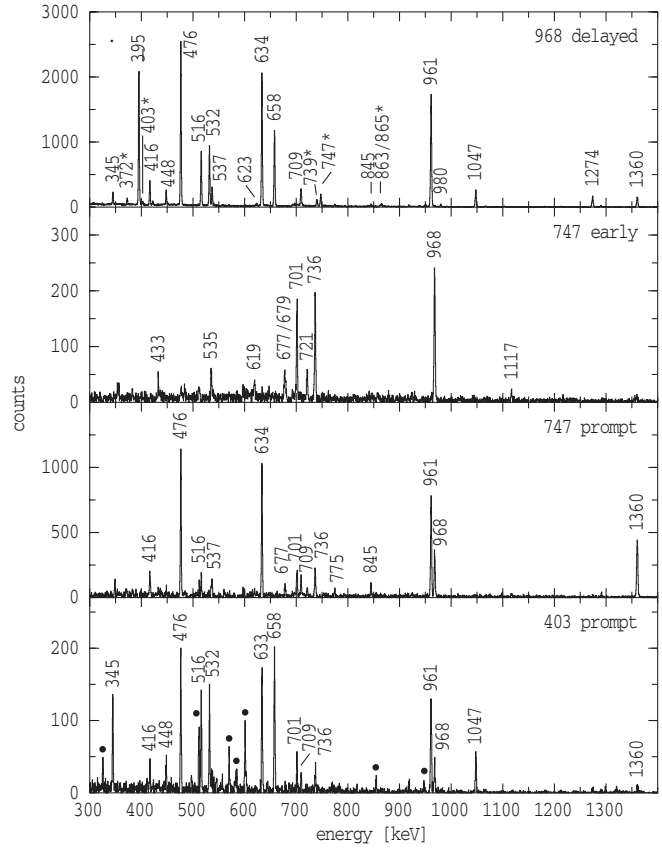

FIG. 4. Time-correlated γ-ray spectra with gates as indicated, selecting transitions directly above and below the 22^+ isomer. (Top) γ rays marked with asterisks are newly assigned transitions that follow the decay of the isomer. Known contaminants are indicated by solid circles.

C. Spin and parity assignments

Assignments were made following consideration of all the available experimental information, including anisotropies, transition strengths, and in some cases, total conversion coefficients. It is not proposed to cover them all in detail, but a number of specific cases that were only briefly covered in Ref. [13] (for states above the 22^+ isomer) require additional substantiation.

The 25^- isomer at 7142 keV was previously established through polarization and conversion coefficient measurements for the 968-keV transition, characterizing it as a stretched octupole [2,3]. In the present measurements, the anisotropy is positive but is not as large as for the case when full alignment is retained, consistent with partial deorientation due to delayed population, predominantly from the 220-ns isomer discussed previously. The 535-keV transition that feeds the 22^+ state has a large negative A_2 coefficient $[-0.50(6)]$, implying a mixed $M1/E2$ dipole transition, and therefore $J^\pi = 23^+$ for the 6709-keV state. The absence of a measurable lifetime would also argue against the alternative $E1/M2$ multipolarity admixture. The 432.5-keV transition has a small positive A_2 coefficient, consistent with a partially deoriented stretched quadrupole, and a delayed intensity balance gives a $\alpha_t = 0.68(8)$, implying $M2$ rather than $E2$ character, giving, independently, 23^+ for the 6709-keV state. The $M2$ strength of 0.14(1) W.u. (Weisskopf units) given in Table II supports the configuration assignment (as discussed later).

Several transitions are now placed parallel to the 7878.3-keV state, which has a firm assignment of $J^\pi = 27^-$. From Table I, the 677.1-keV transition feeding the 25^- state at 7142 keV is seen to have a large negative anisotropy, suggesting a mixed $M1/E2$ transition and $J^\pi = 26^-$ for the 7819.1-keV state. That state decays via the 294.5-keV transition, whose anisotropy is consistent with a stretched dipole character, to the 7524.6-keV state, restricting that state to $J^\pi = 25^\pm$. If one considers the possible transition strengths, the 353.8-keV transition from the 27^- state could be $E2$, but not $M2$, and hence the 25^- assignment to the 7524.6-keV state. Its 382.6-keV decay to the yrast 25^- state has an anisotropy consistent (given some attenuation) with a $J \rightarrow J$ transition, rather than a stretched quadrupole. This is also consistent with the low population of this state. This would be difficult to explain if the 7524.6-keV state had $J^\pi = 27^-$ because the state would then be yrast. The assignments to the 7524.6- and 7819.1-keV states are therefore firm. The other parallel path involves the 720.8-keV transition, which has a well-defined anisotropy and could be a stretched or mixed dipole, suggesting that $J^\pi = 26^\pm$ for the 7862.8-keV state (Table I). However, the implied strength of the (unobserved) 15-keV connecting

TABLE II. Mean lives, branching ratios, and transition strengths for high-lying states in ^{212}Rn. (Results for the 12,211- and 12,548-keV isomeric states are given in Ref. [13].)

Initial state	Final J^π	E_γ (keV)	I_γ relative	$\sigma\lambda$	α_T [20]	$B(E\lambda)$ (e^2 fm$^{2\lambda}$ or μ_0^2 fm$^{(2\lambda-2)}$)	Strength (W.u.)
25^-, 7142 keV, 26(1) ns[a]	23^+	432.5	49(4)	$M2$	0.663	8.3(8)	0.142(13)
	22^+	967.8	1000(10)	$E3$	0.021	$7.68(32) \times 10^4$	28.8(12)
27^-, 7878 keV, 0(1) ns[a]	26^-	(15.5)[b]	0.44(3)	$M1$	153	$6.7(6) \times 10^{-4}$	$4.0(4) \times 10^{-4}$
	26^-	(59.2)[b]	4.5(5)	$M1$	12.8	$1.3(2) \times 10^{-4}$	$7.4(9) \times 10^{-5}$
	25^-	353.8	10.4(30)	$E2$	0.086	$1.6(5) \times 10^{-1}$	$2.2(6) \times 10^{-3}$
	25^-	736.3	322(12)	$E2$	0.015	$1.29(9) \times 10^{-1}$	$1.73(12) \times 10^{-3}$
30^+, 8579 keV, 222(20) ns[a]	(28^+)[c]	(21.9)[b]	0.0031(4)	$E2$	1.28×10^4	5.4(12)	$7.1(16) \times 10^{-2}$
	(28^-)[c]	(21.9)[b]	0.0010(2)	$M2$	4.0×10^4	1.6(4)	2.7(6)
	(28^-)[c]	(21.9)[b]	$1.6(5) \times 10^{-21}$	$E3$	1.53×10^{22}	$1.3(4) \times 10^{-8}$	$4.8(16) \times 10^{-12}$
	28^+	(81.9)[b]	2.1(3)	$E2$	20.7	5.0(9)	$6.1(11) \times 10^{-2}$
	27^-	700.9	322(12)	$E3$	0.0463	$7.24(75) \times 10^4$	27.1(28)
35^-, 11,355 keV, <5 ns[d]	35^-	(92.4)[b]	1.2(2)	$M1$	3.2	$>2.7(7) \times 10^{-4}$	$>1.5(4) \times 10^{-4}$
	(35)	179.3	4.5(5))	$(M1)$	2.50	$>1.4(3) \times 10^{-4}$	$>8(2) \times 10^{-5}$
	34^-	735.1	34.7(20)	$(M1)$	0.054	$>1.5(3) \times 10^{-5}$	$>9(2) \times 10^{-6}$
	33^-	1658.4	7.9(14)	$E2$	0.0033	$>1.6(4) \times 10^{-3}$	$>2.1(6) \times 10^{-5}$

[a]References [1,2].
[b]The γ-ray intensity is implied from the total intensity balance and the theoretical conversion coefficient.
[c]Strengths for alternative spin assignments for the final state are given.
[d]The order of the 179 and 214 cascade transitions is uncertain.

branch from the previous 27^- state would be compatible with $M1$ but not with $E1$, hence leading to the negative parity assignment.

Similar arguments can be applied to the transitions that are now assigned along paths parallel to the 700.9-keV yrast transition, leading to a number of states between the 30^+ and 27^- isomers. One worthy of comment is the 8497.3-keV state assigned as $J^\pi = 28^+$. It decays by a 619.0-keV (attenuated) stretched dipole to the 27^- yrast state and also via the 1355.4-keV transition to the 25^- yrast state. The anisotropy of the 1355-keV transition is consistent with either stretched quadrupole or stretched octupole (and the latter is assigned), but the former would imply $27\hbar$ for the 8497.3-keV state, an assignment that would not be consistent with either the properties of the 619.1-keV transition or the fact that an 82-keV branch from the 30^+ yrast state is observed.

The 8557-keV state is more problematic in that, while its 679-keV dipole decay to the 27^- state and the fact that it is populated via a 22-keV transition from the 30^+ state mean that it must have $J = 28\hbar$, the parity is not defined, although at first, it might seem that the 22-keV transition would have to be $E2$, leading to positive parity. This was the basis of the (28^+) assignment suggested in Ref. [13]. However, as will be discussed in Sec. VI A, further analysis suggests that $E3$ multipolarity (with some $M2$) is possible because of the extremely large conversion coefficients, leading to a (tentative) negative-parity assignment.

Of the states that intervene between the firmly assigned 33^- and 30^+ isomers, the 9446.6-keV state decays by an 867.5-keV transition with a very large negative anisotropy to the 30^+ state, hence leading to the 31^+ assignment given in Ref. [13]. Discrete transitions feeding this state were not identified. Similarly, the 353.7-keV transition that feeds the 30^+ yrast is from a state that has no transitions above it, and its anisotropy [$A_2 = +0.59(14)$] suggests a $J \rightarrow J$ transition, hence leading to the 30^+ assignment to the 8932.9-keV state. The 930.3-keV transition from the 9509.4-keV state is, again, a distinctive mixed dipole [$A_2 = -0.83(6)$; see Table I], leading to the 31^+ assignment to the 9509.4-keV state. In constrast to the other states discussed earlier, it is fed through a complex path, including relatively low energy transitions, a sequence that extends up to connect with the 35^- state at 11,354.6 keV. The ordering of the 179.3- and 214.0-keV transitions in this sequence is not certain, and it has not been possible to make firm spin assignments for a number of the states in this region.

The 34^- and 35^- assignments for the 10,619.5- and 11,354.6-keV states follow from the large anisotropies (Table I) that imply mixed $M1/E2$ character for the 923.7- and 735.1-keV γ rays, as discussed in Ref. [13]. The 642.7-keV transition that feeds the yrast 34^- state also has a distinctive anisotropy, leading to the 35^- assignment for the 11,354.6-keV state and resulting in two 35^- states in fairly close proximity. Both are fed from the 25-ns isomeric state at 12,211.3 keV, the 856.7-keV transition being the dominant branch, and hence the stronger population of the upper 35^- state, rather than the yrast state, presumably because of configuration relationships. These will be discussed in due course. As discussed in Ref. [13], the 856.7-keV transition is either a stretched quadrupole or stretched octupole, leading to the alternatives of $J^\pi = 37^\pm$ or 38^+ for the 12,211.3-keV isomeric state. There are two other branches out of the same state, but neither provides any additional spectroscopic constraint.

TABLE III. Branching ratios and transition strengths for the 22^+ isomer and lower states in ^{212}Rn.

Initial state	Final J^π	E_γ (keV)	I_γ relative	$\sigma\lambda$	α_T [20]	$B(E\lambda)$ (e^2 fm$^{2\lambda}$ or μ_0^2 fm$^{(2\lambda-2)}$)	Strength (W.u.)
11^-, 2761 keV, 8.0(3) ns[a]	10^+	105.8	81.5(28)	$E1$	0.405	$4.33(26) \times 10^{-6}$	$1.89(11) \times 10^{-5}$
	8_2^+	644.5	3.1(6)	$E3$	0.058	$1.18(24) \times 10^5$	44.1(88)
	8_1^+	1066.4	7.0(8)	$E3$	0.0167	$7.8(10) \times 10^3$	2.9(4)
17^-, 4066 keV, 41.7(20) ns[a]	15^-	75.7	20.5(11)	$E2$	30.1	$2.21(19) \times 10^2$	2.94(25)
	14^+	709.1	88.8(42)	$E3$	0.045	$5.67(47) \times 10^4$	21.2(18)
20^+, 5427 keV, 7.5(7) ns[a]	18^+	70	0.54(9)[b]	$E2$	43.7	$2.0(4) \times 10^2$	2.7(5)
	17_2^-	844.5	22.2(42)	$E3$	0.0289	$9.8(2) \times 10^4$	37(8)
	17_1^-	1360.3	124(8)	$E3$	0.0098	$1.95(25) \times 10^4$	7.3(9)
19^-, 5771 keV, <2 ns[c]	20_1^+	344.8	26.7(20)	$E1$	0.0243	$>4.17 \times 10^{-7}$	$>1.8 \times 10^{-7}$
	18^-	657.6	429(10)	$M1$	0.073	$>8.7 \times 10^{-5}$	$>4.9 \times 10^{-5}$
	17^-	1705.1	3.7(6)	$E2$	0.003	$>2.1 \times 10^{-4}$	$>2.8 \times 10^{-6}$
22^+, 6174 keV, 150(4) ns[d]	20_2^+	7.55(30)	$0.64(13) \times 10^{-3}$[b]	$E2$	$6.6(14) \times 10^5$[e]	$2.90(78) \times 10^2$	3.9(10)
	20_1^+	747.3	55.4(28)	$E2$	0.0145	$2.65(49) \times 10^{-3}$	$3.5(7) \times 10^{-5}$
	19^-	402.5	8.1(14)	$E3$	0.258	$1.13(28) \times 10^5$	42(11)

[a]From Ref. [4].
[b]The γ-ray implied intensity from the total intensity balance and the theoretical conversion coefficient.
[c]This work.
[d]Weighted mean of present results and Ref. [21].
[e]Error includes uncertainty in conversion from uncertainty in transition energy.

Three parallel transitions are observed to feed the 12,211.3-keV state. The strongest of these is the 336.3-keV transition, which is a direct decay from the 12-ns isomer at 12,547.6 keV. Its anisotropy suggests a stretched dipole transition, and hence the 12,547.6-keV state must be $1\hbar$ higher in spin than the 12,211.3-keV state. Any further restrictions on the spins and parities of these states rely on a consideration of the transition strengths in conjunction with possible configuration assignments.

IV. TRANSITION STRENGTHS

The $M1$ and $E2$ transition matrix elements for most orbitals in this region are well known (see Refs. [15] and [16] for recent compilations) so that transition rates can be calculated for some of the simpler configurations. Also, it is well known that near $Z = 82$ and $N = 126$, specific proton and neutron orbitals couple strongly to the dominant collective mode, the octupole vibration; hence enhanced $E3$ transitions are common and well studied. They can therefore be used as indicators of specific configuration changes and relationships. In the first instance, "spin-flip" transitions corresponding to an orbital change of either $\nu j_{15/2} \rightarrow \nu i_{11/2}$ or $\pi i_{13/2} \rightarrow \pi h_{9/2}$ are known as type B in the categorization of Ref. [17], for which an $E3$ strength of 3–5 W.u. is expected. Type A transitions are an order of magnitude stronger, ∼20 W.u., and sometimes larger, and they can usually be associated with the $\nu j_{15/2} \rightarrow \nu g_{9/2}$ or $\pi i_{13/2} \rightarrow f_{7/2}$ configuration changes. As shown in detail in a number of publications [3,10,18,19], even larger enhancements are observed because of constructive interference in cases involving both proton and neutron admixtures and configuration changes.

Numerous examples of such enhanced transitions, and also significantly retarded transitions, can be seen in Tables II and III, in which the new experimental results are collected. These will be considered later in the discussion on configuration assignments (Sec. VI).

V. MODEL CALCULATIONS

As indicated in Sec. I, states in ^{212}Rn should be amenable to calculations in a shell-model approach, particularly those formed from valence proton configurations. However, while large-scale shell-model calculations have been reported for the $N = 126$ isotones, these methods are not capable, as yet, of describing states that involve major neutron-core excitations [6,7].

Therefore, to compare with experiment, calculations using the empirical shell model (ESM) were carried out. The structure of selected yrast states in the $N = 126$ nuclei have also been treated by a number of authors within the framework of the DIPM (e.g., Refs. [8,9]). A more comprehensive study including oblate deformation will be considered in Sec. V B.

A. Semiempirical shell model

The ESM calculations are similar to those described in our related work [12,22], which follows the approach outlined originally by Blomqvist [23] and used by several groups (see, e.g., Refs. [24,25]). More detailed explanations are contained in the comprehensive analysis reported for ^{210}Rn in Ref. [12]. In these calculations, within a given configuration, the energy of a basis state depends on the single particle energies and a

weighted sum of two-body interaction matrix elements. While the interactions used are based primarily on the compilation of Lönnroth [26], some cases have been revised recently, as tabulated by Bayer *et al.* [27]. Where possible, empirical interactions were used, rather than calculated values. A departure from this and the earlier compilations of interaction energies is in the choice of values of specific neutron/neutron hole interactions, taken here as $\langle p^{-1}_{1/2} g_{9/2}\rangle = -117$ keV and $\langle p^{-1}_{1/2} j_{15/2}\rangle = -120$ keV. This choice is guided by the analysis and discussion given by Bayer *et al.* [22] for Bi and At cases and corresponds to about half the magnitude of the empirical interactions deduced from ^{208}Pb, a reduction attributed in the ^{208}Pb, 5^- configuration, for example, to blocking of the proton component in the wave function when protons are added. New information on residual interactions obtained from studies of ^{208}Bi [28] has also been incorporated, specifically, the proton/neutron hole interactions $\langle \pi i_{13/2} \nu i^{-1}_{13/2}\rangle_{J=13} = +299$ keV and $\langle \pi i_{13/2} \nu i^{-1}_{13/2}\rangle_{J=12} = +51$ keV.

The only other variation from the values in the appendix of Ref. [27] is for the neutron/neutron hole interaction, $\langle f^{-1}_{5/2} i_{11/2}\rangle_{J=8} = +139$ keV, recently defined through the identification by Heusler *et al.* [29] of the corresponding 8^- state in ^{208}Pb

Diagonalization of the resulting energy matrix gives the excited state energies for each spin belonging to a specific configuration [30]. It should be noted that while mixing between states of the same configuration is calculated correctly, mixing between different configurations is not included. The model space considered in the calculations allows for the distribution of the valence protons over the $h_{9/2}$, $f_{7/2}$, and $i_{13/2}$ orbitals and neutron holes over the $p_{1/2}$, $f_{5/2}$, $p_{3/2}$, and $i_{13/2}$ orbitals. The core excitations considered are those involving promotion of neutrons into the $g_{9/2}, i_{11/2}$, and $j_{15/2}$ orbitals above the shell gap. Core excitation of protons is not usually competitive given the presence of valence protons.

The calculations do not include core polarization effects for configurations in which there is an excitation of neutrons out of the core. From the core polarization strengths used to describe the At nuclei [22], the magnitude of the effect for single-core excitations is expected to be of the order of 50 keV and can probably be ignored given the level of overall uncertainty in the calculations. However, for configurations involving a double-core excitation, the effect could be more significant.

Also, the calculations do not include blocking of the octupole component in cases, for example, in which aligned $g_{9/2}$ and $j_{15/2}$ neutrons are both present, although because empirical interactions are used, part of this effect may already be included in some cases. (The nominal $j_{15/2}$ component, for example, has a large $g_{9/2} \otimes 3^-$ admixture, which is effectively blocked by the addition of an aligned $g_{9/2}$ particle in the multiparticle configuration.) Comments on where these might be significant are included in Tables IV and V.

The results of the calculation are compared with experimental values in Tables IV and V, covering different spin regions, the first corresponding to the region where valence proton configurations dominate and single neutron-core excitations intrude up to spins of $26\hbar$, and the second corresponding to $J \geqslant 27\hbar$, where single and double neutron-core excitations compete, extending into the region of triple core excitations, as reported in Ref. [5].

B. Deformed independent particle model

The DIPM calculations of Andersson *et al.* [8] used the Strutinsky method and the modified harmonic oscillator potential to predict states (specifically yrast traps) up to $30\hbar$. To match the spherical single-particle levels for the $i_{13/2}$ proton and $j_{15/2}$ neutron, they adjusted the parameters given by Nilsson *et al.* [31] to displace those levels through a reduction of the Nilsson parameter μ, and hence the label of the displaced modified oscillator, or DMO. Pairing was not included. The calculations of Matsuyanagi *et al.* [9] were similar in approach but included blocked BCS pairing and a deformed axially symmetric Woods-Saxon potential. The energies of some orbitals were again shifted to match spherical cases. The deformation was determined for each configuration. As well as analyzing yrast isomers up to spin $30\hbar$ to compare with the experimental states known at the time, they also predicted a 35^- yrast trap. Applications to ^{212}Rn and ^{213}Rn using essentially the same approach also were reported in Ref. [5].

This article uses the configuration-constrained approach described elsewhere (see Refs. [32,33]) with a nonaxial Woods-Saxon potential, universal parameters [34], and the Lund convention for specifying the deformation [35]. No modification of the potential has been made, but the Lipkin-Nogami pairing strength has been adjusted to improve the energy matching at sphericity. (See Ref. [36] for some comments on Woods-Saxon potential parameters.) For comparison with the alternative ESM approach, the calculations were carried out for each main (low-lying) configuration either assigned or considered in the ESM calculations. This covers all cases discussed by previous authors and numerous others. As can be seen from the summary given in Table VI, although the triaxial degree of freedom is included, for most configurations, the minimum is found to be close to $\gamma = 60^\circ$, corresponding to oblate deformation. No deformed solution is found for cases involving only valence protons such as the 17^- and 20^+ yrast states. In common with earlier calculations, the magnitude of predicted deformation is generally $|\beta| \leqslant 0.100$, even when extended, as in the present case, to configurations involving triple neutron-core excitations.

Some comments regarding the possible limitations in the DIPM approach are appropriate here. Matsuyanagi *et al.* [9] compared the deformation energy gain for specific configurations with that obtained from the typical residual interactions that are incorporated in the shell model. While for some cases, the deformation energy gain associated with occupying combinations of Nilsson orbitals to produce a given spin roughly mimics the residual interaction in the equivalent shell-model case, there are differences. The most significant of these are that the deformation energy is approximately charge-independent, whereas the shell model interactions are not; there can be oscillations (staggering) as a function of spin

TABLE IV. Calculated (ESM) multiparticle configurations in ^{212}Rn: Part I.

J^π	Proton config.	Neutron config.	E_{calc} (keV)	E_{exp} (keV)	Coupling[a]
0^+	$h^4_{9/2}$	–	193	0	
2^+	$h^4_{9/2}$	–	1393	1274	
4^+	$h^4_{9/2}$	–	1573	1501	
6^+	$h^4_{9/2}$	–	1708	1640	
6^+	$h^4_{9/2}$	–	2248	2306	
8^+	$h^4_{9/2}$	–	1740	1694	
8^+	$h^3_{9/2}f_{7/2}$	–	2085	2116	
8^+	$h^4_{9/2}$	–	2593	(2696)	
9^+	$h^3_{9/2}f_{7/2}$	–	3110		
10^+	$h^4_{9/2}$	–	2632	2655	
10^+	$h^3_{9/2}f_{7/2}$	–	3092	3066	
11^+	$h^3_{9/2}f_{7/2}$	–	3307	3278	
11^-	$h^3_{9/2}i_{13/2}$	–	2728	2761	
12^+	$h^4_{9/2}$	–	2891	2881	m
12^+	$h^3_{9/2}f_{7/2}$	–	3336	3298	
13^+	$h^3_{9/2}f_{7/2}$	–	3473	3510	
13^-	$h^3_{9/2}i_{13/2}$	–	3766	3735	
14^+	$h^3_{9/2}f_{7/2}$	–	3404	3357	
14^-	$h^3_{9/2}i_{13/2}$	–	3994	(3998)	
15^-	$h^3_{9/2}i_{13/2}$	–	4030	3991	
15^-	$h^3_{9/2}i_{13/2}$	–	4141	4151	
16^-	$h^3_{9/2}i_{13/2}$	–	4142	4134	$m-1$
16^-	$h^2_{9/2}f_{7/2}i_{13/2}$	–	4719		
16^-	$h^2_{9/2}f_{7/2}i_{13/2}$	–	4911	(4929)	$m-2$
17^-	$h^3_{9/2}i_{13/2}$	–	4112	4066	m
17^-	$h^2_{9/2}f_{7/2}i_{13/2}$	–	4553	4582	$m-1$
18^+	$h^2_{9/2}i^2_{13/2}$	–	5395	5357	$m-2$
18^-	$h^2_{9/2}f_{7/2}i_{13/2}$	–	5153	5114	m
19^+	$h^2_{9/2}i^2_{13/2}$	–	5670	5795	$m-1$
19^-	$h^3_{9/2}f_{7/2}$	$p^{-1}_{1/2}g_{9/2}$	5760	5771	m
20^+	$(h^2_{9/2}i^2_{13/2})_{20^+}$	–	5425	5427	m
20^+	$h^3_{9/2}i_{13/2}$	$p^{-1}_{1/2}g_{9/2}$	5998	6167	$m-2$
22^+	$(h^3_{9/2}i_{13/2})_{17^-}$	$p^{-1}_{1/2}g_{9/2}$	6037	6174	m
23^+	$h^3_{9/2}i_{13/2}$	$f^{-1}_{5/2}g_{9/2}$	6723	6822	$m-1$
23^+	$(h^2_{9/2}f_{7/2}i_{13/2})_{18^-}$	$p^{-1}_{1/2}g_{9/2}$	6752		m
23^+	$(h^3_{9/2}i_{13/2})_{17^-}$	$p^{-1}_{1/2}i_{11/2}$	6799	6709	m
24^+	$(h^3_{9/2}i_{13/2})_{17^-}$	$f^{-1}_{5/2}g_{9/2}$	7082	7178	m
25^-	$(h^2_{9/2}i^2_{13/2})_{20^+}$	$p^{-1}_{1/2}g_{9/2}$	6987[b]	7142	m
25^-	$(h^3_{9/2}i_{13/2})_{17^-}$	$p^{-1}_{1/2}j_{15/2}$	7226[b]	7525	m
26^-	$(h^2_{9/2}i^2_{13/2})$	$f^{-1}_{5/2}g_{9/2}$	7704	7819	$m-1$
26^-	$(h^2_{9/2}i^2_{13/2})_{20^+}$	$p^{-1}_{3/2}g_{9/2}$	7963	7863	m
26^-	$(h^3_{9/2}i_{13/2})_{17^-}$	$f^{-1}_{5/2}j_{15/2}$	7967	$m-1$	

[a]Coupling is indicated by m for maximum.

[b]Multiple-octupole mixed configurations.

TABLE V. Calculated multiparticle configurations (ESM) in ^{212}Rn: Part II.

J^π	Proton config.	Neutron config.	$E_{\rm calc}$ (keV)	$E_{\rm exp}$ (keV)	Coupling[a]
27^-	$(h^2_{9/2}i^2_{13/2})_{20^+}$	$f^{-1}_{5/2}g_{9/2}$	8166[b]		m
27^-	$(h^3_{9/2}i_{13/2})_{17^-}$	$p^{-2}_{1/2}g_{9/2}i_{11/2}$	8178	7878	m
27^-	$(h^3_{9/2}i_{13/2})_{17^-}$	$f^{-1}_{5/2}j_{15/2}$	8351[b]	8362	m
28^+	$(h^2_{9/2}i^2_{13/2})_{20^+}$	$p^{-1}_{1/2}j_{15/2}$	8260	8497	m
28^-	$(h^2_{9/2}f_{7/2}i_{13/2})_{18^-}$	$p^{-2}_{1/2}g_{9/2}i_{11/2}$	8670	(8557)	m
29^+	$(h^3_{9/2}i_{13/2})_{17^-}$	$p^{-2}_{1/2}g_{9/2}j_{15/2}$	8890	9028	m
29^+	$(h^2_{9/2}i^2_{13/2})$	$i^{-1}_{13/2}g_{9/2}$	8979		$m-2$
29^+	$(h^2_{9/2}i^2_{13/2})_{20^+}$	$f^{-1}_{5/2}j_{15/2}$	9027		m
29^-	$(h^3_{9/2}i_{13/2})$	$p^{-1}_{1/2}f^{-1}_{5/2}g_{9/2}i_{11/2}$	9154		$m-1$
30^+	$(h^2_{9/2}i^2_{13/2})_{20^+}$	$p^{-2}_{1/2}g_{9/2}i_{11/2}$	9105[b]	8579	m
30^+	$(h^3_{9/2}i_{13/2})_{17^-}$	$p^{-2}_{1/2}i_{11/2}j_{15/2}$	9263[b]	8933	m
31^+	$(h^2_{9/2}i^2_{13/2})$	$p^{-1}_{1/2}f^{-1}_{5/2}g_{9/2}i_{11/2}$	9796	9447	$m-2$
31^+	$(h^3_{9/2}i_{13/2})$	$p^{-1}_{1/2}f^{-1}_{5/2}g_{9/2}j_{15/2}$	9885	9510	$m-1$
31^-	$(h^2_{9/2}i^2_{13/2})$	$p^{-2}_{1/2}g_{9/2}j_{15/2}$	9785	(9609)	$m-1$
32^-	$(h^2_{9/2}i^2_{13/2})_{20^+}$	$p^{-2}_{1/2}g_{9/2}j_{15/2}$	9572[c]		m
32^-	$(h^2_{9/2}i^2_{13/2})$	$i^{-1}_{13/2}j_{15/2}$	10,350	(10,103)	$m-1$
32^+	$(h^2_{9/2}i^2_{13/2})$	$p^{-1}_{1/2}f^{-1}_{5/2}g_{9/2}i_{11/2}$	10,107	(10,125)	$m-1$
32^+	$(h^3_{9/2}i_{13/2})$	$p^{-1}_{1/2}f^{-1}_{5/2}i_{11/2}j_{15/2}$	10,315		$m-1$
32^+	$(h^2_{9/2}i^2_{13/2})_{20^+}$	$p^{-1}_{1/2}p^{-1}_{3/2}g_{9/2}i_{11/2}$	10,323		m
33^-	$(h^2_{9/2}i^2_{13/2})_{20^+}$	$p^{-2}_{1/2}i_{11/2}j_{15/2}$	10,274	9696	m
33^-	$(h^2_{9/2}i^2_{13/2})$	$p^{-1}_{1/2}f^{-1}_{5/2}g_{9/2}j_{15/2}$	10,346		$m-2$
34^-	$(h^2_{9/2}i^2_{13/2})$	$p^{-1}_{1/2}f^{-1}_{5/2}g_{9/2}j_{15/2}$	10,589	10,620	$m-1$
34^-	$(h^2_{9/2}i^2_{13/2})_{20^+}$	$p^{-1}_{1/2}p^{-1}_{3/2}g_{9/2}j_{15/2}$	10,781[c]	(11,086)	m
34^+	$(h^3_{9/2}i_{13/2})_{17^-}$	$f^{-2}_{5/2}i_{11/2}j_{15/2}$	11,188	(11,176)	m
34^+	$(h^2_{9/2}i^2_{13/2})_{20^+}$	$f^{-2}_{5/2}g_{9/2}i_{11/2}$	11,401	(11,176)	m
35^-	$(h^2_{9/2}i^2_{13/2})$	$p^{-1}_{1/2}f^{-1}_{5/2}g_{9/2}j_{15/2}$	11,299	11,262 (or 11,355)	m
35^-	$(h^2_{9/2}i^2_{13/2})$	$p^{-1}_{1/2}f^{-1}_{5/2}i_{11/2}j_{15/2}$	11,350	11,355 (or 11,262)	$m-1$
35^-	$(h^2_{9/2}i^2_{13/2})$	$p^{-1}_{1/2}i^{-1}_{13/2}g_{9/2}i_{11/2}$	11,502	(11,463)	$m-2$
35^-	$(h^3_{9/2}i_{13/2})$	$p^{-2}_{1/2}f^{-1}_{5/2}g_{9/2}i_{11/2}j_{15/2}$	11,517		$m-2$
35^+	$(h^2_{9/2}i^2_{13/2})$	$p^{-1}_{1/2}f^{-1}_{5/2}j^2_{15/2}$	12,041	(11,880)	$m-2$
36^-	$(h^3_{9/2}i_{13/2})$	$p^{-2}_{1/2}f^{-1}_{5/2}g_{9/2}i_{11/2}j_{15/2}$	11,542	(11,671)	$m-1$
36^+	$(h^2_{9/2}i^2_{13/2})$	$p^{-2}_{1/2}f^{-1}_{5/2}g^2_{9/2}j_{15/2}$	12,160	(11,828)	$m-2$
37^-	$(h^2_{9/2}f_{7/2}i_{13/2})$	$p^{-2}_{1/2}f^{-1}_{5/2}g_{9/2}i_{11/2}j_{15/2}$	12,033	12,211	$m-1$
37^+	$(h^2_{9/2}i^2_{13/2})$	$p^{-1}_{1/2}i^{-1}_{13/2}g_{9/2}j_{15/2}$	11,941	(12,053)	$m-2$
37^+	$(h^2_{9/2}i^2_{13/2})$	$p^{-2}_{1/2}f^{-1}_{5/2}g^2_{9/2}j_{15/2}$	12,256		$m-1$
38^+	$(h^2_{9/2}i^2_{13/2})$	$p^{-2}_{1/2}f^{-1}_{5/2}g_{9/2}i_{11/2}j_{15/2}$	12,136	12,548	$m-2$
39^+	$(h^2_{9/2}i^2_{13/2})$	$p^{-2}_{1/2}f^{-1}_{5/2}g_{9/2}i_{11/2}j_{15/2}$	12,213		$m-1$
39^+	$(h^2_{9/2}i^2_{13/2})$	$f^{-1}_{1/2}i^{-1}_{13/2}g_{9/2}j_{15/2}$	13,199		$m-3$
39^+	$(h^2_{9/2}i^2_{13/2})$	$p^{-2}_{1/2}f^{-1}_{5/2}g_{9/2}i_{11/2}j_{15/2}$	13,250		$m-1$
40^+	$(h^2_{9/2}i^2_{13/2})_{20^+}$	$p^{-2}_{1/2}f^{-1}_{5/2}g_{9/2}i_{11/2}j_{15/2}$	12,949[c]		m

[a]Coupling indicated by m for maximum.
[b]Configurations will be mixed.
[c]Energy will be underestimated because of neglect of octupole blocking.

TABLE VI. Multiparticle configurations in ^{212}Rn calculated on a deformed basis.

J^π	Proton config.	Neutron config.	β_2	β_4	γ	$E_{\rm calc}$ (keV)	$E_{\rm calc}$ (keV)[a]
20^+	$(h^2_{9/2}i^2_{13/2})_{20^+}$		<0.04				
20^+	$(h^3_{9/2}i_{13/2})_{17^-}$	$(p^{-1}_{1/2}g_{9/2})_{3^-}$	<0.04				
20^+	$(h^3_{9/2}i_{13/2})_{15^-}$	$(p^{-1}_{1/2}g_{9/2})_{5^-}$	<0.04				
22^+	$(h^3_{9/2}i_{13/2})_{17^-}$	$(p^{-1}_{1/2}g_{9/2})_{5^-}$	0.049	−0.018	60	7395	6174[a]
23^+	$(h^2_{9/2}f_{7/2}i_{13/2})_{18^-}$	$(p^{-1}_{1/2}g_{9/2})_{5^-}$	0.055	0.007	60	7267	6046
23^+	$(h^3_{9/2}i_{13/2})_{17^-}$	$(f^{-1}_{5/2}g_{9/2})_{6^-}$	<0.04				
23^+	$(h^3_{9/2}i_{13/2})_{17^-}$	$(p^{-1}_{1/2}i_{11/2})_{6^-}$	0.053	−0.013	60	7871	6650
24^+	$(h^3_{9/2}i_{13/2})_{17^-}$	$(f^{-1}_{5/2}g_{9/2})_{7^-}$	<0.04				
25^-	$(h^2_{9/2}i^2_{13/2})_{20^+}$	$(p^{-1}_{1/2}g_{9/2})_{5^-}$	0.057	−0.016	60	8540	7319
25^-	$(h^3_{9/2}i_{13/2})_{17^-}$	$(p^{-1}_{1/2}j_{15/2})_{8^+}$	0.052	−0.012	60	8438	7217
26^-	$(h^2_{9/2}i^2_{13/2})_{20^+}$	$(f^{-1}_{5/2}g_{9/2})_{6^-}$	0.052	−0.003	47	9546	8325
26^-	$(h^2_{9/2}i^2_{13/2})_{20^+}$	$(p^{-1}_{1/2}i_{11/2})_{6^-}$	0.060	−0.012	59	8981	7760
27^-	$(h^3_{9/2}i_{13/2})_{17^-}$	$(p^{-2}_{1/2}g_{9/2}i_{11/2})_{10^+}$	0.078	−0.019	60	9314	8093
28^+	$(h^2_{9/2}i^2_{13/2})_{20^+}$	$(p^{-1}_{1/2}j_{15/2})_{8^+}$	0.060	−0.010	60	9548	8327
28^-	$(h^2_{9/2}f_{7/2}i_{13/2})_{18^-}$	$(p^{-2}_{1/2}g_{9/2}i_{11/2})_{10^+}$	0.081	0.005	60	9031	7810
29^-	$(h^3_{9/2}i_{13/2})_{17^-}$	$(p^{-1}_{1/2}f^{-1}_{5/2}g_{9/2}i_{11/2})_{12^+}$	0.067	0.002	48	10,786	9565
30^+	$(h^2_{9/2}i^2_{13/2})_{20^+}$	$(p^{-2}_{1/2}g_{9/2}i_{11/2})_{10^+}$	0.082	0.004	60	9783	8562
30^+	$(h^3_{9/2}i_{13/2})_{17^-}$	$(p^{-2}_{1/2}i_{11/2}j_{15/2})_{13^-}$	0.080	−0.013	60	10,283	9062
30^+	$(h^2_{9/2}f_{7/2}i_{13/2})_{18^-}$	$(p^{-2}_{1/2}g_{9/2}j_{15/2})_{12^-}$	0.080	0.007	60	9585	8364
31^+	$(h^2_{9/2}i^2_{13/2})_{20^+}$	$(p^{-1}_{1/2}f^{-1}_{5/2}g_{9/2}i_{11/2})_{11^+}$	0.066	−0.002	51	11,945	10,724
31^+	$(h^3_{9/2}i_{13/2})_{17^-}$	$(p^{-1}_{1/2}f^{-1}_{5/2}g_{9/2}j_{15/2})_{14^-}$	0.068	0.004	50	11,350	10,129
32^-	$(h^2_{9/2}i^2_{13/2})_{20^+}$	$(p^{-2}_{1/2}g_{9/2}j_{15/2})_{12^-}$	0.085	−0.016	60	10,800	9579
33^-	$(h^2_{9/2}i^2_{13/2})_{20^+}$	$(p^{-2}_{1/2}i_{11/2}j_{15/2})_{13^-}$	0.084	0.008	60	10,656	9435
34^-	$(h^2_{9/2}i^2_{13/2})_{20^+}$	$(p^{-1}_{1/2}f^{-1}_{5/2}g_{9/2}j_{15/2})_{14^-}$	0.075	0.005	60	12,316	11,095
35^-	$(h^2_{9/2}i^2_{13/2})_{20^+}$	$(p^{-1}_{1/2}f^{-1}_{5/2}g_{9/2}j_{15/2})_{15^-}$	0.066	0.000	60	13,147	11,926
35^-	$(h^2_{9/2}i^2_{13/2})_{20^+}$	$(p^{-1}_{1/2}f^{-1}_{5/2}i_{11/2}j_{15/2})_{15^-}$	0.079	0.010	56	12,633	11,412
37^-	$(h^2_{9/2}f_{7/2}i_{13/2})_{18^-}$	$(p^{-2}_{1/2}f^{-1}_{5/2}g_{9/2}i_{11/2}j_{15/2})_{19^+}$	0.103	0.014	57	12,977	10,857
38^+	$(h^2_{9/2}i^2_{13/2})_{20^+}$	$(p^{-2}_{1/2}f^{-1}_{5/2}g_{9/2}i_{11/2}j_{15/2})_{18^+}$	0.085	0.000	60	15,110	13,889
39^+	$(h^2_{9/2}i^2_{13/2})_{20^+}$	$(p^{-2}_{1/2}f^{-1}_{5/2}g_{9/2}i_{11/2}j_{15/2})_{19^+}$	0.089	0.004	60	14,705	13,484
40^+	$(h^2_{9/2}i^2_{13/2})_{20^+}$	$(p^{-2}_{1/2}f^{-1}_{5/2}g_{9/2}i_{11/2}j_{15/2})_{20^+}$	0.094	0.016	60	14,084	12,863

[a]Energies shifted down by 1221 keV to match the 22^+ yrast state.

in a multiplet, which do not occur in the deformed cases, and in no cases does the deformation produce the strong repulsion that is evident particularly in configurations associated with mutually aligned high-spin proton particles and neutron holes [37]. As well, the absolute accuracy expected in the deformed models is ∼1–2 MeV, although relative energies should be considerably better. Given these qualifications, the expectation (as articulated in Refs. [8,9]) was that the DIPM would be most appropriate for configurations with aligned particles and non-aligned neutron holes and would not, in general, be valid for couplings to nonmaximal spins. Evidently, such calculations will miss cases in which repulsion due to the (shell-model) residual interactions is important. The hope expressed in these studies was that with equal numbers of aligned proton particles and neutron particles, the isospin dependence retained in the shell model would be washed out and therefore be less problematic.

Overall, it was also found previously that the energies calculated for configurations involving only valence particle configurations were underestimated, whereas the energies of core excited states were generally overestimated.

The results of the present DIPM calculations are summarized in Table VI. Unmodified energies are given in the penultimate column, whereas the last column gives the energies shifted down by 1221 keV so that the predicted and observed 22^+ state energies match. These and the ESM results will be compared to experimental results in the following section.

VI. RESULTS AND DISCUSSION

A. Transition strengths and configuration assignments

Stuchbery *et al.* [4] measured the lifetime of the 11^- yrast state from the (seniority-two) $\pi h^3_{9/2}i_{13/2}$ valence configuration,

whose main decay is via a 106-keV $E1$ branch, while a 1067-keV $E3$ branch to the 8_1^+ state was assigned by Lönnroth *et al.* [5], albeit with an approximate intensity. As indicated in Table I, we have confirmed this branch and also observed the 644.5-keV $E3$ branch to the 8_2^+ state, defining both intensities. The 8^+ states are from the nominal $h_{9/2}^2$ and $h_{9/2}f_{7/2}$ configurations, although they are expected to be partly mixed. Nevertheless, the $E3$ decay strengths (Table III) fall into the categories of type A and type B enhanced $E3$ transitions discussed earlier.

No new branches are observed from the 17^- state at 4066 keV, but the branching intensities have been more precisely determined. The decay is through the enhanced $E2$ transition of 76 keV and an enhanced 709-keV $E3$ transition (type A), in good agreement with the expectations for the configuration changes (Table IV) and with the quantitative estimates given in Ref. [4].

The 19^- state at 5771 keV is short-lived, with an experimental limit of $\tau < 2$ ns. A new, relatively high energy branch of 1705 keV to the 17^- yrast has been observed, but from Table III, it can be seen that the three branches from the state are not significantly constrained by the upper lifetime limit, being in the range $>10^{-4}$ to 10^{-6} W.u. Nevertheless, it should be noted that this state is the first single neutron-core excitation in the spectrum (Table IV), and all decays to the purely valence proton configurations could be expected to be inhibited, as is the case for some higher states (to be discussed later).

New branches have been observed for the decay of the 20^+ isomer at 5427 keV, formed from the $\pi h_{9/2}^2 i_{13/2}^2$ valence protons—essentially the maximum spin that can be expected using only protons near the Fermi surface. Its decays mimic, to some extent, those of the 17^- state, with an enhanced $E2$ transition [2.7(5) W.u.; Table III] to the 18^+ state from the lower spin coupling of the same configuration and two enhanced $E3$ transitions, one of type A and one of type B, in excellent agreement with the configuration assignments to the initial 20^+ state and to the two lower 17^- states (Table IV).

This consistency is carried through to the properties of the 22^+ isomer at 6174 keV, whose branches (and energy) were reported in Ref. [13]. The 7.6-keV $E2$ transition to the yrare 20^+ state is enhanced [3.9(10) W.u.], consistent with the states being members of the same multiplet. In contrast, the 747-keV $E2$ to the yrast 20^+ state formed by valence protons is highly retarded, with a strength of only $3.5(7) \times 10^{-5}$ W.u. This retardation can be taken as characteristic of decays between core excited and noncore excited states involving significant orbital changes. The decay of the 23^+ isomer in ^{210}Rn [12] is a similar example, with two $E2$ decays with strengths of 4.2×10^{-4} and 7.0×10^{-6} W.u., resulting in an isomer with a relatively long lifetime. The third branch from the 22^+ state identified is an enhanced $E3$ transition with a strength of $\sim$42 W.u., a type A transition owing effectively to the proton $i_{13/2} \rightarrow f_{7/2}$ transition, confirming the configuration assignments of both initial and final states.

The configuration of the 25^- isomeric state at 7142 keV has previously been established from a variety of spectroscopic information, including its enhanced $E3$ decay and measured g factor, as a mixture of the two competing core-excited configurations $\pi h_{9/2}^2 i_{13/2}^2 \times \nu p_{1/2}^{-1} g_{9/2}$ and $\pi h_{9/2}^3 i_{13/2} \times \nu p_{1/2}^{-1} j_{15/2}$. The complementary partner is presumably the newly assigned 25^- state at 7525 keV, and a 433-keV $M2$ branch is observed to a 23^+ state at 6709 keV. The $M2$ strength of 0.14(1) W.u. supports the association of the 6709-keV state with the $\pi h_{9/2}^3 i_{13/2} \times \nu p_{1/2}^{-1} j_{11/2}$ configuration predicted at 6799 keV. The configuration change from the 25^- state corresponds to a neutron $j_{15/2} \rightarrow i_{11/2}$ transition from one component of the mixed 25^- state wave function. The $\nu j_{15/2} \rightarrow i_{11/2}$ transition is known from ^{209}Pb to have a strength of 0.55(14) W.u. [38]. By default, a second 23^+ state observed at 6821 keV, to which the 25^- state does not decay, could be associated with either the $\pi h_{9/2}^3 i_{13/2} \times \nu f_{5/2}^{-1} g_{9/2}$ $(m-1)$ or the $\pi h_{9/2}^2 f_{7/2} i_{13/2} \times \nu p_{1/2}^{-1} g_{9/2}$ configuration, even though both are predicted at slightly lower energies: 6723 and 6752 keV, respectively. Assignment to the former configuration is proposed because that allows the association of the 24^+ state at 7178 keV, which only decays to the 6821-keV, 23^+ state, as the maximum coupling (m) of the same configuration. The energy difference of 356 keV is indicative of the repulsive neutron-proton interaction that is present when the $f_{5/2}$ neutron hole is maximally aligned with the protons. This assignment for the 23^+ state is also supported by the observation of a mixed $M1/E2$ transition (647.2 keV) to the 22^+ yrast state because these states would then be closely related, essentially by a $f_{5/2}^{-1} \rightarrow p_{1/2}^{-1}$ neutron transition.

The next stage in the scheme is the decay of the 27^- isomeric state at 7878 keV. The scheme reported in Ref. [13] has 354- and 736-keV $E2$ branches to both 25^- states discussed previously. As can be seen from Table II, the $E2$ strengths are essentially the same, consistent with the identification of the 25^- states as being mixed. The strengths are also low, at $\sim 1 \times 10^{-3}$ W.u., consistent with a decay from the $\pi h_{9/2}^3 i_{13/2} \times \nu p_{1/2}^{-2} g_{9/2} i_{11/2}$ (m) double core-excited configuration assigned (Table V) to a single core excitation. The two low-energy $M1$ branches from the 27^- state to the 7819- and 7862-keV states are even weaker, at $\sim 10^{-4}$ W.u., consistent, again, with significant configuration changes, in this case (see Table IV) a change from a double to a single core excitation in the neutron component and a change (in shorthand notation) from a $[h^3 i; 17^-]$ to a $[h^2 i^2; 20^+]$ configuration in the protons. (As noted elsewhere, $E2$ strengths between states that involve multiple orbital changes can be expected to lead to hindrances of $\sim 10^5$.)

The 30^+, 222-ns isomer at the 8579-keV state has an enhanced $E3$ decay (and measured g factors) that define its mixed double neutron-core excited configuration and its relationship to the configuration of the 27^- state, as discussed extensively elsewhere [3,10]. Two low-energy $E2$ branches are also observed here: These are both weak but are not as inhibited as those observed in the decay of the 27^- state. The configuration assignment to the 28^+ state (fed by the 82-keV transition) is firm because it decays by a 1355-keV $E3$ transition to the 7142-keV 25^- state, which has a related configuration. As noted earlier, the 8557-keV state that is fed via the 22-keV transition has $J = 28$, but its parity is not certain. While an $E2$ assignment to the 22-keV

transition seems logical, the second 28^+ state predicted in the calculations is about 500 keV higher. However, a 28^- state is expected in this energy region (at 8670 keV). A 28^- assignment would imply $M2$ or $E3$ character for the 22-keV transition. This is not as unlikely as might first be thought because of the large conversion coefficients for such low energies. From Table II, a pure $M2$ transition would be a factor of about 10 too strong at 2.7(6) W.u., but because the conversion coefficient for an $E3$ transition is extremely high ($>10^{22}$), the corresponding $E3$ γ-ray strength is very low. An $M2/E3$ transition is therefore plausible, leading to a possible 28^- state at an energy that is in good agreement with the prediction. The predicted state has a double core-excited configuration, and its decay to the 27^- state (single core-excited) would involve several orbital changes among both protons and neutrons. The 679-keV transition shows no evidence for $E2$ admixtures, consistent with this proposition.

No new branches were observed from the 33^- isomer, which has a single enhanced $E3$ decay. It is populated from the newly assigned, short-lived 34^- state at 10,620 keV via the 924-keV transition. Both states are double core excitations with the same proton component and similar neutron configurations, consistent with the absence of a significant lifetime for the 34^- state. Its lifetime limit (conservatively, <5 ns) corresponds to strengths of $\geqslant 10^{-6}$ W.u. or $\geqslant 10^{-3}$ W.u. for $M1$ and $E2$ multipolarities for the 924-keV transition [which, from the large anisotropy of $A_2 = -0.73(6)$, is probably mixed]. The situation is similar for the 35^- state at 11,355 keV: It has a number of branches and has been assigned as the first triple neutron-core excitation, which would imply relatively hindered transitions to the lower states. The lifetime limit corresponds to lower limits of $\sim 10^{-4}$–10^{-5} W.u. for all branches, so it is neither a constraint nor a support for the assignment.

The possible spin assignments and implied decay transition strengths for two highest lying isomers identified in this study were discussed at some length in Ref. [13] and will not be repeated here.

B. ESM results and excitation energies

The agreement in excitation energy between the ESM and experiment in the spin region below about $22\hbar$ is very good, as can be seen in Table IV and Fig. 5. As is expected, the 0^+ ground-state depression is underestimated by nearly 200 keV (a similar discrepancy is seen for the ground state of ^{213}Fr [19]), but essentially all other states predicted to lie near the yrast line are observed with energies reproduced to better than 100 keV, and many within 50 keV, over the whole spin range for the valence proton configurations. While no candidate is observed for the theoretical 9^+ state from the $\pi h_{9/2}^3 f_{7/2}$ configuration, it is predicted to be significantly above the yrast line; hence it is unlikely to be populated directly. This is also the case for the 21^- state from the $\pi h_{9/2} i_{13/2}^3$ configuration, which is calculated to lie at about 7.2 MeV, over 1 MeV above the yrast line. There are two other 21^- states and a 21^+ state that are predicted to be lower, specifically at 6098, 6369, and

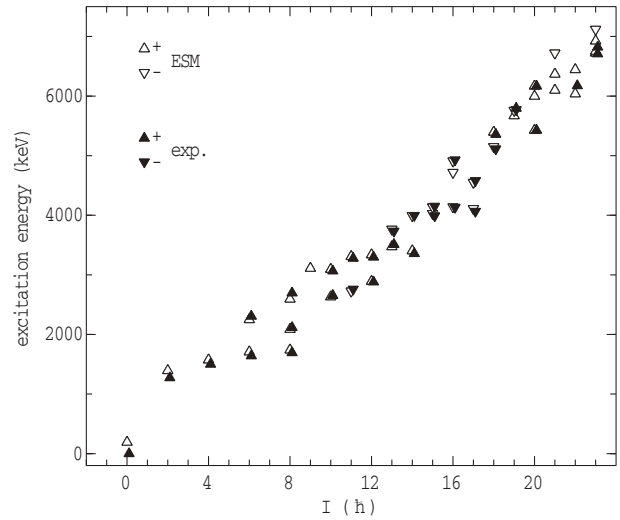

FIG. 5. Comparison between experimental and predicted states up to spins of about $24\hbar$. Only states predicted to lie near the yrast line are shown.

6723 keV, all arising from single neutron-core excitations, for which there are no experimental counterparts. (Because of space limitations, these are included in Fig. 5 but not in Table IV.) Because of their nonyrast nature, they might not be strongly populated, but they would probably have preferential decays to the 19^- core-excited state at 5771 keV or, by retarded transitions, to the yrast 20^+ state at 5427 keV.

Several other comments are appropriate: As indicated earlier, the state observed at 2696 keV has been assumed to be the third 8^+ state, although it does not have a firm spin assignment. Similarly, the 3998-keV experimental state has been associated with the predicted 14^- state at 3993 keV, again without a firm spin assignment. (These are included in parentheses in Table IV.) Also, there are two (nonyrast) 16^- states predicted at 4719 and 4911 keV, both arising from the $\pi h_{9/2}^2 f_{7/2} i_{13/2}$ configuration, but only one candidate experimental state is observed at 4929 keV. Although nonyrast, it is preferentially populated by an $E3$ decay from the proposed 19^+ state at 5795 keV, consistent with the implied configuration change. The absence of a similar decay to a lower (predicted) state could be because of phase differences in the wave functions for the 16^- states, with destructive interference resulting for one of the possible $E3$ transitions.

The only experimental state for which we do not have a theoretical counterpart is the proposed state at 2967 keV, which was identified in Ref. [4] with a single decay (206.6 keV) to the 11^- yrast state. We do not observe any new transitions that would substantiate this placement and assignment, but also, we cannot disprove it. (The present experimental conditions would result in a lower population of nonyrast states than found in Ref. [4].)

C. ESM and DIPM results: $J \geqslant 24\hbar$

In the higher spin region (see Table V and Ref. [13]), associating predicted states with the observed spectrum is more complicated because, in general, the level density is higher.

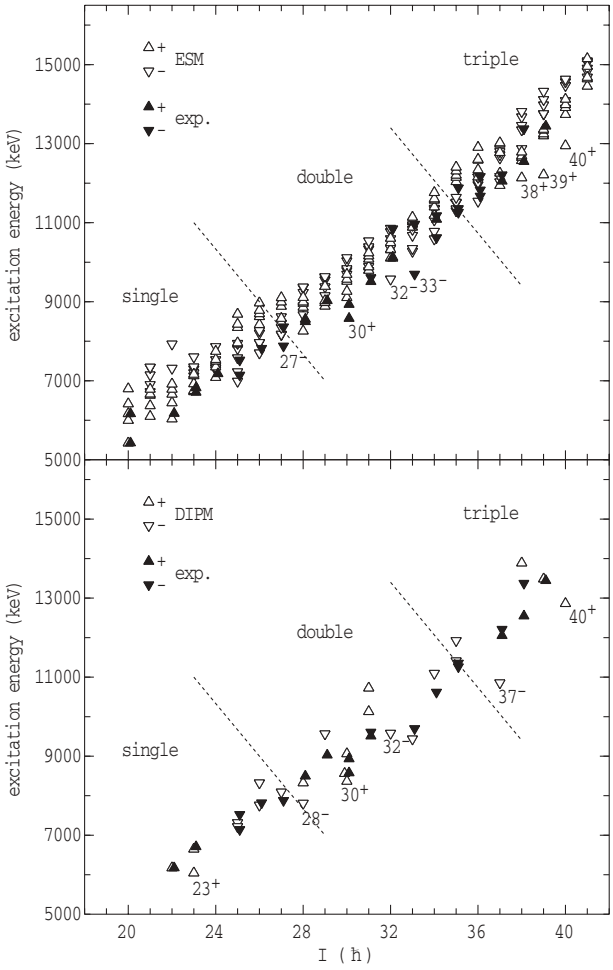

FIG. 6. Comparison between experimental and predicted states between $20\hbar$ and $40\hbar$, as predicted (top) from the ESM calculations (adapted from Ref. [13]) and (bottom) the DIPM calculations (from this article). Note that only selected states have been calculated in the latter case, and the energies have been shifted downward by 1221 keV to match the 22^+ states. Specific states of interest discussed in the text are marked. The dashed lines demarcate approximately the regions of single, double, and triple neutron-core excitations.

As can be seen from Table V, many of the states that fall near the yrast line involve nonmaximal couplings [as indicated by the notation (m), $(m-1)$, etc.]. This results in competing configurations being close in energy, a situation rather different to that which pertains in higher Z nuclei, where a few particular combinations tend to dominate the yrast line. The increased level density is apparent in the comparison given in Fig. 6 (top). Specific assignments and ambiguities that arise were covered in some detail in Ref. [13], so the main emphasis in the present case will be on the comparison with the predictions of the DIPM, to be discussed in a subsequent section. The DIPM results are reproduced in Fig. 6 (bottom).

D. Core excitation, deformation, and assigned configurations

As outlined earlier, the historical development of the understanding of the structure of high-spin isomers in ^{212}Rn initially involved a shell-model perspective and then models incorporating (oblate) deformation. While there were common assignments for many configurations, different configurations were suggested for a number of the key states. At the time of the review of de Voigt *et al.* [39], the multiparticle configurations based on the predictions of the DIPM were mostly in agreement with each other and were generally accepted, although there remained some differences between the results.

However, a number of those assignments were questioned, both before that review and after (see, e.g., Refs. [3,10,40]), because they were incompatible with the experimental feature of enhanced $E3$ transitions between states such as the 30^+ and 27^- pair in ^{212}Rn (and the related $63/2^-$ and $57/2^+$ pair in ^{211}Rn). The enhanced decay meant that whatever the structure of the upper state, the state to which it decayed would have to have a closely related configuration.

In ^{212}Rn, for example, the DIPM and DMO assignments for the 30^+ and 27^- states in ^{212}Rn were associated with the following configurations:

(i) for 30^+,

$$\pi\left(h_{9/2}^2 f_{7/2} i_{13/2}\right)_{18^-} \nu\left(p_{1/2}^{-2} g_{9/2} j_{15/2}\right)_{12^-},$$
$$\beta \sim -0.095(\epsilon_2 = -0.10);$$

(ii) for 27^-,

$$\pi\left(h_{9/2}^3 i_{13/2}\right)_{17^-} \nu\left(p_{1/2}^{-2} g_{9/2} i_{11/2}\right)_{10^+},$$
$$\beta \sim -0.070(\epsilon_2 = -0.08).$$

From simple angular momentum coupling restrictions, and given the number of orbital changes required, an $E3$ transition between such configurations is essentially forbidden. The problem is compounded because an enhanced $33^- \rightarrow 30^+$ transition is also observed, severely constraining the configuration of three states in sequence. Similar arguments apply to the $69/2^+ \rightarrow 63/2^- \rightarrow 57/2^+$ sequence in ^{211}Rn [3].

As discussed earlier, the deformation energy in the DIPM accounts for a considerable portion of the shell-model interaction, but it is not precisely equivalent, the difference being configuration-dependent. (A direct comparison of deformation energy and residual interactions for the configuration proposed for the 30^+ isomer in ^{212}Rn is given in Ref. [41].) Andersson *et al.* [8] showed that inclusion of the deformation in their DMO model dramatically improved the comparison between theory and experiment, compared to a pure "spherical" case. However, this improvement in energy should not be taken to imply that deformation is a necessary component, and it can be misleading if the configuration assignments disagree with other experimental properties.

A second problem that confronts the DIPM interpretation is the small quadrupole moment measured for the $63/2^-$ isomer in ^{211}Rn [42]. Its magnitude can be explained by the mixed shell-model configurations, without requiring significant deformation [42]. A similar conclusion was reached [43] from the measurement of the quadrupole moment in ^{213}Fr$_{126}$, which has a related configuration, and from the theoretical analysis given by Sagawa and Arima [44] for a number of high-spin isomers in the Pb region.

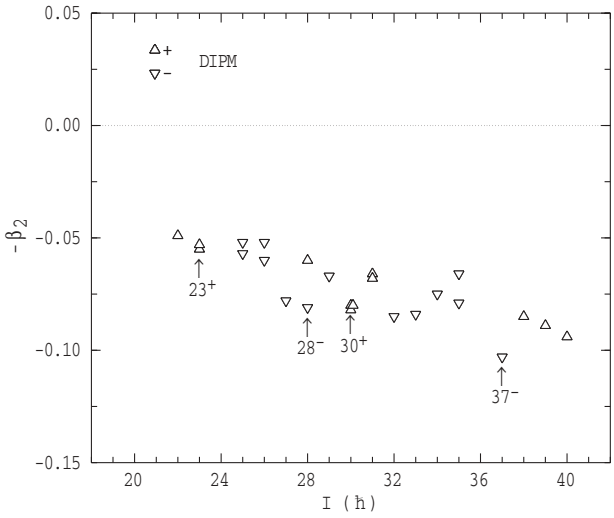

FIG. 7. Equilibrium quadrupole deformations from the DIPM model for the states given in Table VI. Note that all have small values of β_4 and $\gamma \approxeq 60^\circ$. The arrows mark states that have the common 18^- proton component, as discussed in the text. Note also that the calculations use the Lund convention; hence, for $\gamma = 60^\circ$, the β_2 parameter is of opposite sign to β or ϵ_2 in the other DIPM calculations discussed in the text.

It should be noted that while the magnitude of the deformation predicted by the calculations becomes larger as more neutron-core excitations occur, it remains in the region of $\leqslant 0.10$. The trend can be seen in Fig. 7. Only the quadrupole deformation is plotted, given that the higher multipoles are small and the triaxiality parameter γ is close to 60° for all calculated states.

From a detailed comparison of the two approaches depicted in Fig. 6 (with numerical values given in Tables IV and V and VI), a number of key points emerge. As discussed earlier, while the energy of the lowest 30^+ state in the deformed calculations matches experimental values, its configuration is inconsistent with the observed decays. The calculated 30^+_2 and 30^+_3 (DIPM) states are, in fact, the ones that correspond to the two lowest ESM states (which mix), whose properties match experimental results. The 23^+, 28^-, 30^+_1, and 37^- states marked in Fig. 6 (bottom) in the deformed calculation, in fact, all fall relatively low in energy. From Table VI, it can be seen that these have a common component from the $(h^2_{9/2} f_{7/2} i_{13/2})_{18^-}$ proton configuration, the only core-excited states with such a component. In all cases, except perhaps for the 30^+_1 state, these also all have a predicted deformation that is equal to or larger than other configurations in the same region, particularly the 37^- state. We are led to conclude that in the DIPM, the energies of the states involving the 18^- proton configuration are underestimated. This seems to be the source of the original discrepancy between the DIPM configuration assignments and the shell-model assignments for the 30^+ isomer, a conclusion that can be reached now that a more extensive comparison has been possible.

The yrast trap with $J^\pi = 35^-$ predicted by Matsuyanagi *et al.* [9] was from the $J_{\max} - 3$ coupling from the $\pi(h^2_{9/2} f_{7/2} i_{13/2})_{18^-} \nu p^{-2}_{1/2} f^{-1}_{5/2} g_{9/2} i_{11/2} j_{15/2}$ configuration, involving both the 18^- proton component and a triple neutron-core excitation. However, this is not the same configuration as that assigned here (from the ESM) to either of the observed 35^- states.

In addition to the limitations in the DIPM outlined earlier, another factor that could have a bearing on the difference between the predictions is the neglect of spin-spin interactions in the deformed case. These have a significant effect in the energies of high-K states, causing relative shifts of several hundred keV [45]. Writing the Nilsson configurations for the main states with the intrinsic spin couplings explicit gives

30^+_1(DIPM);
$\pi 9/2^-[505\downarrow]7/2^-[514\downarrow]7/2^-[503\downarrow]13/2^+[606\uparrow]$
$\otimes\ \nu 9/2^+[615\downarrow]15/2^-[615\uparrow]$,

30^+_2(DIPM);
$\pi 9/2^-[505\downarrow]7/2^-[514\downarrow]13/2^+[606\uparrow]11/2^+[615\uparrow]$
$\otimes\ \nu 9/2^+[615\downarrow]11/2^+[606\downarrow]$.

In terms of the generalized Gallagher-Moszkowski splittings [45], there are four antiparallel proton-neutron couplings ($[\uparrow\downarrow, \downarrow\uparrow]$) in the first configuration and eight parallel couplings ($[\uparrow\uparrow, \downarrow\downarrow]$) in the second. There are corresponding differences in the neutron-neutron and proton-proton couplings as well, and depending on the magnitudes of the (configuration-dependent) interactions, there is likely to be a significant difference in the total residual interaction for the two cases. Unfortunately, few of the interactions are known empirically because these orbital combinations do not generally arise in prolate deformed nuclei, the source of most of the empirical data. However, schematically, it would seem that the first configuration would be more depressed in energy than the second, thus exacerbating, rather than resolving, the discrepancy.

Another state of interest in the comparison between the ESM and DIPM calculations is a 32^- state from the same configuration predicted at essentially the same energy in both calculations (9572 keV in the ESM model and 9579 keV in the DIPM model), for which there is no experimental counterpart. The predicted energy in the ESM will be underestimated in this case because it neglects octupole blocking. The 33^- experimental state at 9696 keV is predicted at 9435 keV in the DIPM, a better match than the value of 10,274 keV from the ESM, but the ESM fares better for the (possible) yrast 38^+ state. Finally, both calculations predict a low-lying 40^+ state at essentially the same energy, 12,949 keV in the ESM and 12,863 keV in the DIPM, a state for which no candidate has been observed. As concluded in Ref. [13], the nonobservation of this state, which is likely to be an isomer, is surprising.

To conclude, it appears that the ESM provides a more reliable approach to the characterization of observed high-spin states in ^{212}Rn, with the qualification that there remain ambiguities about the more complicated triple neutron-core excitations. By implication, a similar judgment could be reached for nearby Rn isotopes. In contrast, the predictability of the DIPM calculations is open to question, with a consistent mismatch between apparent agreements in energy for favored

states and the configuration relationships implied by the detailed decay properties.

The DIPM has also been applied to another region where (oblate) high-spin isomeric states occur, specifically, close to the $Z = 64$ subshell and $N = 82$ shell closures (see, e.g., Refs. [39,46], and references therein). This region differs in principle from the Rn region in that the nuclei are softer, and purportedly larger oblate deformations ($\beta_2 \sim -0.2$) occur. These are driven largely by the $d_{3/2}$ neutron holes and $d_{5/2}$ proton holes created in core excitations, the proton and neutron gaps being similar and smaller than in the Rn region. Nevertheless, there are considerable similarities in the competing shell-model multiparticle excitations, and significant octupole coupling is present. Spin and parity assignments for the high-lying isomers are rarely unambiguous and often rely partly on predictions of the DIPM (e.g., Ref. [47]). It remains to be seen whether such deformed configuration assignments are consistent with the relationships between the initial (isomeric) state and the final states.

VII. SUMMARY

A comprehensive level scheme has been established for the $N = 126$ nuclide ^{212}Rn. New states with firm spin assignments and new γ-ray branches have been assigned in the scheme up to $J \sim 20\hbar$, a region where most states are formed from couplings of the four valence protons. The precise energy and decay properties of the yrast $22\hbar$ isomer have also been defined, confirming its spin and parity and configuration. The semiempirical shell model succeeds in accounting for nearly all such states observed, with predicted energies that agree, relatively precisely, with experimental values. An extensive level scheme is also established for the higher spin region, up to $J \sim 39\hbar$, with an excitation energy in excess of 13 MeV, covering states formed by aligned valence protons combined with single, double, and triple neutron-core excitations. Calculations within both the shell-model framework and the deformed independent particle model have been carried out, with mixed success. Most of the states can be described within the ESM, albeit without the precision found for the lower spin, less complex configurations. While the DIPM has some success in describing the relative energies of the main yrast states, predicting them to have oblate shapes with relatively small deformations, some of the agreement is superficial in that the configuration assignments are inconsistent with the decay properties, particularly the enhanced $E3$ transitions observed. This discrepancy has been pointed out before, but the present, more extensive calculations suggest that the discrepancy can be traced to an underestimate of the energy of the 18^- proton configuration in the deformed space. Both calculations also predict a relatively low energy (yrast) 40^+ state, which, as yet, has not been identified. Progress in this area, particularly with the ESM, is likely to require self-consistent incorporation of octupole coupling effects, core polarization, Pauli blocking, and possible modification of the residual interactions.

ACKNOWLEDGMENTS

The authors thank the academic and technical staff of the Heavy Ion Accelerator Facility for their continuing support. P.N. was partly supported by funding from the Academy of Finland under Grant No. 121110.

[1] D. Horn, O. Häusser, T. Faestermann, A. B. McDonald, T. K. Alexander, J. R. Beene, and C. J. Herrlander, Phys. Rev. Lett. **39**, 389 (1977).
[2] D. Horn, O. Häusser, B. Hass, T. K. Alexander, T. Faestermann, H. R. Andrews, and D. Ward, Nucl. Phys. **A317**, 520 (1979).
[3] G. D. Dracoulis, P. M. Davidson, A. P. Byrne, B. Fabricius, T. Kibèdi, A. M. Baxter, A. E. Stuchbery, A. R. Poletti, and K. J. Schiffer, Phys. Lett. **B246**, 31 (1990).
[4] A. E. Stuchbery, G. D. Dracoulis, A. P. Byrne, and A. R. Poletti, Nucl. Phys. **A486**, 397 (1988).
[5] T. Lönnroth, C. W. Beausang, D. B. Fossan, L. Hildingsso, W. F. Piel Jr., and E. K. Warburton, Phys. Scr. **39**, 56 (1989).
[6] L. Coraggio, A. Covello, A. Gargano, N. Itaco, and T. T. S. Kuo, Phys. Rev. C **60**, 064306 (1999).
[7] E. Caurier, M. Rejmund, and H. Grawe, Phys. Rev. C **67**, 054310 (2003).
[8] C. G. Andersson *et al.*, Nucl. Phys. **A309**, 141 (1978).
[9] K. Matsuyanagi, T. Dossing, and K. Neergard, Nucl. Phys. **A307**, 253 (1978).
[10] S. J. Poletti, G. D. Dracoulis, A. R. Poletti, A. P. Byrne, A. E. Stuchbery, and J. Gerl, Nucl. Phys. **A448**, 189 (1986).
[11] P. M. Davidson, G. D. Dracoulis, A. P. Byrne, T. Kibèdi, B. Fabricius, A. M. Baxter, A. E. Stuchbery, A. R. Poletti, and K. J. Schiffer, Nucl. Phys. **A560**, 822 (1993).
[12] A. R. Poletti, A. P. Byrne, G. D. Dracoulis, T. Kibèdi, and P. M. Davidson, Nucl. Phys. **A756**, 83 (2005).
[13] G. D. Dracoulis, G. J. Lane, A. P. Byrne, P. M. Davidson, T. Kibédi, P. Nieminen, K. H. Maier, H. Watanabe, and A. N. Wilson, Phys. Lett. **B662**, 19 (2008).
[14] G. D. Dracoulis, G. J. Lane, A. P. Byrne, P. M. Davidson, T. Kibédi, P. Nieminen, K. H. Maier, H. Watanabe, and A. N. Wilson, Phys. Rev. C **77**, 034308 (2008).
[15] M. Rejmund, M. Schramm, and K. H. Maier, Phys. Rev. C **59**, 2520 (1999).
[16] K. H. Maier *et al.*, Phys. Rev. C **76**, 064304 (2007).
[17] I. Bergström and B. Fant, Phys. Scr. **31**, 26 (1985).
[18] A. R. Poletti, G. D. Dracoulis, A. P. Byrne, A. E. Stuchbery, S. J. Poletti, G. Gerl, and P. M. Lewis, Phys. Lett. **B154**, 263 (1985).
[19] A. P. Byrne, G. D. Dracoulis, C. Fahlander, H. Hübel, A. R. Poletti, A. E. Stuchbery, J. Gerl, R. F. Davie, and S. J. Poletti, Nucl. Phys. **A448**, 137 (1986).
[20] T. Kibédi, T. W. Burrows, M. B. Trzhaskovskaya, P. M. Davidson, and C. J. Nestor Jr., Nucl. Instrum. Methods A **589**, 202 (2008).
[21] E. Browne, Nucl. Data Sheets **104**, 427 (2005).
[22] S. Bayer, A. P. Byrne, G. D. Dracoulis, A. M. Baxter, T. Kibèdi, and F. G. Kondev, Nucl. Phys. **A694**, 3 (2001).
[23] J. Blomqvist, in *Proceedings of the Argonne Symposium on High Spin Phenomena in Nuclei*, ANL/PHY-79-4 (Argonne National Laboratory, Argonne, Illinois, 1979), p. 155.

[24] V. Rahkonen, I. Bergström, J. Blomqvist, O. Knuuttila, K.-G. Rensfelt, J. Sztarkier, and K. Westerborg, Z. Phys. A **284**, 357 (1978).
[25] M. Rejmund *et al.*, Eur. Phys. J. A **1**, 261 (1998).
[26] T. Lönnroth, Experimental and theoretical two-nucleon interaction energies in the lead region, Dept. of Physics, University of Jyväskylä, RR 4/81 (unpublished).
[27] S. Bayer, A. P. Byrne, G. D. Dracoulis, A. M. Baxter, T. Kibèdi, F. G. Kondev, S. M. Mullins, and T. R. McGoram, Nucl. Phys. **A650**, 3 (1999).
[28] B. Fornal *et al.*, Phys. Rev. C **67**, 034318 (2003).
[29] A. Heusler *et al.*, Phys. Rev. C **74**, 034303 (2006).
[30] P. M. Davidson, Australian National University Department of Nuclear Physics Internal Report No. P1636, 2005 (unpublished).
[31] S. G. Nilsson *et al.*, Nucl. Phys. **A131**, 1 (1969).
[32] F. R. Xu, P. M. Walker, and J. A. Sheikh, Phys. Lett. **B435**, 257 (1998).
[33] F. R. Xu, Chin. Phys. Lett. **18**, 750 (2001).
[34] W. Nazarewicz, J. Dudek, R. Bengtsson, T. Bengtsson, and I. Ragnarsson, Nucl. Phys. **A435**, 397 (1985).
[35] G. Andersson, S. E. Larsson, G. Leander, P. Möller, S. G. Nilsson, I. Ragnarsson, and S. Åberg, Nucl. Phys. **A268**, 205 (1976).
[36] J. Dudek, Z. Szymański, and T. Werner, Phys. Rev. C **23**, 920 (1981).
[37] J. P. Schiffer and W. W. True, Rev. Mod. Phys. **48**, 191 (1976).
[38] M. J. Martin, Nucl. Data Sheets **22**, 545 (1977).
[39] M. J. A. de Voigt, J. Dudek, and Z. Szymański, Rev. Mod. Phys. **55**, 949 (1983).
[40] G. D. Dracoulis, C. Fahlander, and A. R. Poletti, Phys. Rev. C **24**, 2386 (1981).
[41] A. P. Byrne and G. D. Dracoulis, Nucl. Phys. **A391**, 1 (1982).
[42] E. Dafni, M. Hass, E. Naim, M. H. Rafailovich, A. Berger, H. Grawe, and H.-E. Mahnke, Phys. Rev. Lett. **55**, 1269 (1985).
[43] A. P. Byrne, R. Müsseler, H. Hübel, K. H. Maier, and H. Kluge, Nucl. Phys. **A516**, 145 (1990).
[44] H. Sagawa and A. Arima, Phys. Lett. **B202**, 15 (1988).
[45] K. Jain, O. Burglin, G. D. Dracoulis, B. Fabricius, N. Rowley, and P. M. Walker, Nucl. Phys. **A591**, 61 (1995).
[46] Y. Gono *et al.*, Eur. Phys. J. A **13**, 5 (2002).
[47] T. Fukuchi *et al.*, Eur. Phys. J. A **39**, 49 (2009).